

24 an NMB of -8.8%. PM_{2.5} concentrations are moderately overpredicted with an NMB of 23.3% at
25 rural sites, but slightly underpredicted with an NMB of -10.8% at urban/suburban sites. In general,
26 the model performs relatively well for chemical and meteorological variables, and not as well for
27 aerosol-cloud-radiation variables. Cloud-aerosol variables including aerosol optical depth, cloud
28 water path, cloud optical thickness, and cloud droplet number concentration are generally
29 underpredicted on average across the continental U.S. Overpredictions of several cloud variables
30 over eastern U.S. result in underpredictions of radiation variables (such as GSW with an MB of -
31 5.7 W m⁻²) and overpredictions of shortwave and longwave cloud forcing (MBs of ~7 to 8 W m⁻²)
32 which are important climate variables. While the current performance is deemed to be acceptable,
33 improvements to the bias-correction method for CESM downscaling and the model
34 parameterizations of cloud dynamics and thermodynamics, as well as aerosol-cloud interactions
35 can potentially improve model performance for long-term climate simulations.

36 **KEYWORDS:** Online-Coupled WRF/Chem; Climate, Air Quality, the Representative
37 Concentration Pathway Scenarios, Climatological Evaluation; Chemistry-Climate Interactions

38 **1. Introduction**

39 Regional atmospheric models have been developed and applied for high resolution climate,
40 meteorology, and air quality modeling in the past few decades. Comparing to global models with
41 a coarser domain resolution (Leung et al., 2003) those regional models have advantages over
42 global models because they can more accurately represent mesoscale variability (Feser et al.,
43 2011), and also better predict the local variability of concentrations of specific species such as
44 black carbon and sulfate (Petikainen et al., 2012). General circulation models (GCMs) and global
45 chemical transport models (GCTMs) are usually downscaled to regional meteorological models
46 such as the Weather Research and Forecasting model (WRF) (Caldwell et al., 2009; Gao et al.,

47 2012), regional climate models such as REMO-HAM (Petikainen et al., 2012), the regional
48 modeling system known as Providing Regional Climates for Impacts Studies (PRECIS) (Jones et
49 al., 2004; Fan et al., 2014), and a number of European models described in Jacob et al. (2007), as
50 well as regional CTMs such as the Community Multiscale Air Quality Model (CMAQ) (Penrod et
51 al., 2014; Xing et al., 2015). These regional models are used for climate/meteorology or air quality
52 simulations. Some are applied for more than ten years (Caldwell et al., 2009; Warrach-Sagi et al.,
53 2013; Xing et al., 2015). However these regional models either lack the detailed treatment of
54 chemistry (e.g., in WRF), or use prescribed chemical concentrations (e.g., REMO-HAM uses
55 monthly mean oxidant fields for several chemical species), or do not have online-coupled
56 meteorology and chemistry (e.g., in CMAQ). In addition, the past regional model simulations and
57 analyses have mainly focused on meteorological parameters such as surface temperature and
58 precipitation, cloud variables such as net radiative cloud forcing, and chemical constituents such
59 as ozone. Regional climate model simulations tend to focus on significant climatic events such as
60 extreme temperatures (very cold or very hot) (Dasari et al., 2014), heat waves, heavy precipitation,
61 drought, and storms (Beniston et al., 2007), rather than the important air quality and climate
62 interactions. In addition, the impacts of complex chemistry-aerosol-cloud-radiation-climate
63 feedbacks on future climate change remain uncertain, and these feedbacks are most accurately
64 represented using online-coupled meteorology and chemistry models (Zhang, 2010; IPCC, 2013).
65 An online-coupled meteorology and chemistry model, however, is more computationally
66 expensive compared to an offline-coupled model (Grell et al., 2004), and thus requires significant
67 computing resources for their long-term (a decade or longer) applications. With rapid increases in
68 the availability of high performance computing resources on the petaflop scale, however, long
69 term simulations using online-coupled models have become possible in recent years. For example,

70 recently, the WRF model has been coupled online to the CMAQ model with the inclusion of
71 aerosol indirect effects to study chemistry and climate interactions (Yu et al., 2014).

72 The online-coupled WRF model with Chemistry (WRF/Chem) has been updated with a
73 suite of physical parameterizations from the Community Atmosphere Model version 5 (CAM5)
74 (Neale et al., 2010) so that the physics in the global CAM5 model is consistent with the regional
75 model for downscaling purposes (Ma et al., 2014). There are also limited applications of dynamical
76 downscaling (Gao et al., 2013) under the new Intergovernmental Panel on Climate Change (IPCC)
77 Fifth Assessment Report's Representative Concentration Pathway (RCP) scenarios (van Vuuren
78 et al., 2011). Gao et al. (2013) applied dynamic downscaling to link the global-climate-chemistry
79 model CAM-Chem with WRF and CMAQ using RCP 8.5 and RCP 4.5 emissions to study the
80 impacts of climate change and emissions on ozone (O₃). Molders et al. (2014) downscaled the
81 Community Earth System Model (CESM) (Hurrell et al., 2013) to drive the online-coupled
82 WRF/Chem model over Southeast Alaska using RCP 4.5 emissions; however, their study did not
83 address the feedback processes between chemistry and meteorology. This study evaluates the
84 online-coupled regional WRF/Chem model, which takes into account gas and aerosol-phase
85 chemistry, as well as aerosol direct and indirect effects. WRF/Chem is used to simulate the
86 "current" climate scenario for 10 years, from 2001 to 2010 using the RCP 8.5 emissions and
87 boundary conditions from an updated version of CESM with advanced chemistry and aerosol
88 treatments over continental U.S. (CONUS) (He et al., 2015; Glotfelty et al., 2015) with a focus on
89 air-quality and climate interactions. Both CESM and WRF/Chem include similar gas-phase
90 chemistry and aerosol treatments. To our best knowledge, this study is the first to report the
91 WRF/Chem simulation, evaluation, and analyses over a period of 10 years (i.e., 2001-2010) to
92 assess if the model is able to accurately simulate decadal long air quality and climatology by taking

93 into account feedback processes between chemistry and meteorology. This study also assesses
94 whether the RCP8.5 emissions for the 10-year period are robust enough to produce satisfactory
95 performance against observations with WRF/Chem.

96 **2. Model Set-up and Evaluation Protocol**

97 **2.1 Model Configurations and Simulation Design**

98 The model used is the modified WRF/Chem v3.6.1 with updates similar to those
99 implemented into WRF/Chem v3.4.1 as documented in Wang et al. (2014). The main updates
100 include the implementation of an extended version of Carbon Bond 2005 (CB05) (Yarwood et al.,
101 2005) gas-phase mechanism with the chlorine chemistry (Sarwar et al., 2007) and its coupling with
102 the Modal for Aerosol Dynamics in Europe/Volatility Basis Set (MADE/VBS) (Ahmadov et al.,
103 2012). MADE/VBS incorporates a modal aerosol size distribution, and includes an advanced
104 secondary organic aerosol (SOA) treatment based on gas-particle partitioning and gas-phase
105 oxidation in volatility bins. The CB05-MADE/VBS option has also been coupled to existing model
106 treatments of various feedback processes such as the aerosol semi-direct effect on photolysis rates
107 of major gases, and the aerosol indirect effect on cloud droplet number concentration (CDNC) and
108 resulting impacts on shortwave radiation. The main physics and chemistry options used in this
109 study as well as their corresponding references can be found in Table 1. The simulations are
110 performed at a horizontal resolution of 36-km with 148×112 horizontal grid cells over the
111 CONUS domain and parts of Canada and Mexico, and a vertical resolution of 34 layers from the
112 surface to 100-hPa. Considering the decadal applications of WRF/Chem in this work which is
113 much longer than many past WRF/Chem applications, the simulations are reinitialized monthly
114 (rather than 1-4 days used in most past WRF/Chem applications to short-term episodes that are on
115 an order of months up to 1-year, e.g., Zhang et al., 2012a, b; Yahya et al., 2014, 2015b) to constrain

116 meteorological fields toward National Centers for Environmental Prediction (NCEP) reanalysis
117 data while allowing chemistry-meteorology feedbacks within the system. As discussed in Sections
118 3.1 and 3.3, the reinitialization frequency of 1-month may be too large to constrain some of the
119 meteorological fields such as moistures, which in turn affect other parameters, and a more frequent
120 reinitialization may be needed to improve the model performance. The impact of the frequency of
121 the reinitialization on simulated meteorological and cloud parameters will be further discussed in
122 Sections 3.1 and 3.2. A list of acronyms used in this paper can be found in Table S1.

123 **2.2 Processing of Emissions and Initial Conditions (ICs)/Boundary Conditions (BCs)**

124 Global RCP emissions are available as monthly-average emissions for 2000, 2005, and for
125 every 10 years between 2010 and 2100, at a grid resolution of $0.5^{\circ} \times 0.5^{\circ}$ (Moss et al., 2010; van
126 Vuuren et al., 2011). The RCP emissions in 2000, 2005, and 2010 are used to cover the 10-year
127 emissions needed for WRF/Chem simulations, i.e., the periods of 2001 – 2003, 2004 – 2006, and
128 2007 – 2010, respectively. Processing global RCP emissions in 2000, 2005, and 2010 into regional,
129 hourly emissions needed for the 10-year WRF/Chem simulations requires essentially three main
130 tasks. These include 1) mapping the RCP species to CB05 speciation used in WRF/Chem; 2) re-
131 gridding the RCP emissions from $0.5 \times 0.5^{\circ}$ grid resolution to the 36×36 km grid resolution used
132 for regional simulation over North America; and 3) applying species and location dependent
133 temporal allocations (i.e., emissions variation over time) to the re-gridded RCP emissions. Table
134 S2 shows the species mapping between RCP species and CB05 species. To map the RCP species
135 to CB05 speciation, some assumptions are made due the relatively detailed speciation required by
136 CB05. Some of the CB05 species are directly available in RCP; however, others are lumped into
137 RCP groups, for example, the “other alkanals” and “hexanes and higher alkanes” in the RCP
138 groups can be considered to approximately represent the acetaldehyde and higher aldehydes

139 emissions required by CB05, respectively (Table S2). For the CB05 species such as ethanol,
140 methanol, internal and terminal olefin carbon bonds in the gas-phase, and elemental and organic
141 carbon in the accumulation mode of the aerosol particles, other RCP groups are used to
142 approximate these emissions (Table S2). For the remaining CB05 species that are not available in
143 RCP (i.e. chlorine, HCl, HONO, NH_4^+ , NO_3^- , PAR, unspciated $\text{PM}_{2.5}$, H_2SO_4 , and SO_4^{2-}), their
144 2000 emissions are based on the 2002 National Emission Inventory (NEI) (version 3,
145 <http://www.epa.gov/ttn/chief/emch/>), while their 2005 and 2010 emissions are based on the 2008
146 NEI-derived emissions (version 2) from the Air Quality Modelling Evaluation International
147 Initiative (AQMEII) project as described in Pouliot et al. (2015), which include year-specific
148 updates for on/off road transport, wildfires and prescribed fires, and Continuous Emission
149 Monitoring-equipped point sources. To re-grid the RCP emissions, the RCP rectilinear grid is first
150 interpolated to a WRF/Chem curvilinear grid using a simple inverse distance weighting (NCAR
151 Command Language Function – `rgrid2rcm`), and a subset of the RCP grid that covers the
152 WRF/Chem CONUS domain is then extracted. To derive a temporal allocation for monthly-
153 averaged RCP emissions, hourly emission profiles are taken from those used in-house WRF/Chem
154 simulations over CONUS during 2001 (Yahya et al., 2015a), and 2006 and 2010 as part of the
155 AQMEII project (Yahya et al., 2014, 2015b). The emissions for those existing in-house
156 simulations were generated based on the 2002 NEI, the emissions were generated with the Sparse
157 Matrix Operator Kernel Emissions (SMOKE) model version 2.3. The emissions for the existing
158 in-house 2006 and 2010 simulations were generated based on the pre-merged emissions provided
159 by the U.S. EPA, which were derived from the 2008 NEI with year-specific section emissions for
160 2006 and 2010 as part of the AQMEII. SMOKE version 3.4 was used to prepare the spatially,
161 temporally, and chemically speciated “model-ready” emissions for the existing in-house 2006 and

162 2010 WRF/Chem simulations. Since NEI is updated and released every three years, the temporal
 163 profiles of emissions used in SMOKE for 2002, 2006 and 2010 are assumed to be valid for 3-4
 164 years around the NEI years, i.e., 2001-2003, 2004-2006, and 2007-2010, respectively. The
 165 temporal allocations applied to the RCP emissions are therefore based on the SMOKE model's
 166 profiles for each species and source location, and include non-steady-state emissions rates (i.e.,
 167 seasonal, weekday or weekend, and diurnal variability) that are valid for the entire simulation
 168 periods of 2001-2010. Specifically, the hourly re-gridded RCP emission rates for each species E ,
 169 or E_{hr}^{RCP} are calculated by

$$170 \quad E_{hr}^{RCP}(t, z, lat, lon) = E_{mon}^{RCP}(z, lat, lon) * \left[\frac{E_{hr}^{WRF}(t, z, lat, lon)}{E_{mon}^{WRF}(z, lat, lon)} \right] \quad (1)$$

171 where E_{mon}^{RCP} , E_{mon}^{WRF} , and E_{hr}^{WRF} represent the original monthly-averaged RCP emissions rates, the
 172 monthly-averaged WRF/Chem emissions rates, and the hourly WRF/Chem emission rates,
 173 respectively, which are valid at each model time t , layer z , and lat and lon grid points. The RCP
 174 elevated source emissions for sulfur dioxide (SO₂), sulfate (SO₄²⁻), elemental carbon (EC) and
 175 organic carbon (OC) were also incorporated into the model-ready emissions for WRF/Chem using
 176 steps 1) – 3) and Eq. (1) above. Lastly, RCP aircraft source emissions for EC, nitric oxide (NO),
 177 and nitrogen dioxide (NO₂) are directly injected into the closest model layers. No temporal
 178 allocations are applied to the RCP aircraft source emissions.

179 Biogenic emissions are calculated online using the Model of Emissions of Gases and
 180 Aerosols from Nature version 2 (MEGAN2) (Guenther et al., 2006). Emissions from dust are based
 181 on the online Atmospheric and Environmental Research Inc. and Air Force Weather Agency
 182 (AER/AFWA) scheme (Jones and Creighton, 2011). Emissions from sea salt are generated based
 183 on the scheme of Gong et al. (1997).

184 The chemical and meteorological ICs/BCs come from the modified CESM/CAM5 version
185 1.2.2 with updates by He et al. (2014) and Glotfelty et al. (2015) developed at the North Carolina
186 State University (CESM_NCSU). WRF/Chem and CESM both use the CB05 gas-phase
187 mechanism (Yarwood et al., 2005), however, WRF/Chem includes additional chlorine chemistry
188 from Sarwar et al. (2007), whereas CESM_NCSU uses a modified version of CB05, the CB05
189 Global Extension (CB05GE) by Karamchandani et al. (2012). In addition to original reactions in
190 CB05 and chlorine chemistry of Sarwar et al. (2007), CB05GE includes chemistry on the lower
191 stratosphere, reactions involving mercury species, and additional heterogeneous reactions on
192 aerosol particles, cloud droplets and on polar stratospheric clouds (PSCs). Both WRF/Chem and
193 CESM_NCSU use a modal aerosol size representation, rather than a sectional size representation.
194 While WRF/Chem includes MADE/VBS with 3 prognostic modes (Ahmadov et al.,
195 2012),CESM_NCSU includes the Modal Aerosol Model with 7 prognostic modes (Liu et al., 2012)
196 is used in CESM_NCSU. In addition to similar gas-phase chemistry and aerosol treatments,
197 CESM_NCSU and WRF/Chem use the same shortwave and longwave radiation schemes (i.e., the
198 Rapid and accurate Radiative Transfer Model for GCM (RRTMG)), though they use different
199 cloud microphysics parameterizations, PBL, and convection schemes. As GCMs generally contain
200 systematic biases which can influence the downscaled simulation, the meteorological ICs/BCs
201 predicted by CESM_NCSU are bias corrected before they are used by WRF/Chem using the
202 simple bias correction technique based on Xu and Yang (2012). Temperature, water vapor,
203 geopotential height, wind, and soil moisture variables available every 6 hours from the NCEP Final
204 Reanalyses (NCEP FNL) dataset are used to correct the ICs and BCs derived based on results from
205 CESM_NCSU for WRF/Chem simulations. In this bias-correction approach, monthly
206 climatological averages for ICs and BCs are first derived from both NCEP and CESM_NCSU

207 cases. The differences between the ICs and BCs from the NCEP and CESM_NCSU climatological
 208 averages are then added onto the CESM_NCSU ICs and BCs to generate bias-corrected
 209 CESM_NCSU ICs/BCs. Assuming that the causes for the biases remain the same in future, this
 210 bias correction technique can also be applied to future year simulations for which NCEP FNL data
 211 is not available.

212 **2.3 Model Evaluation Protocol**

213 The focus of the model evaluation is mainly to assess whether the model is able to
 214 adequately reproduce the spatial and temporal distributions of key meteorological and chemical
 215 variables as compared to observations on a climatological time scale. A scientific question to be
 216 addressed in this work is, is WRF/Chem sufficiently good for regional climate and air quality
 217 simulations on a decadal scale? A climatological month refers to the average of the month for all
 218 the 10 years. For example, January refers to the average for all the months of January from 2001
 219 to 2010. Statistical evaluations such as mean bias (MB), Pearson’s correlation coefficient (R),
 220 normalized mean bias (NMB), normalized mean error (NME) (The definition of those measures
 221 can be found in Yu et al. (2006) and Zhang et al. (2006)) and Index of Agreement (IOA) ranging
 222 from 0 to 1 (Willmott et al., 1981) for major chemical and meteorological variables are included.
 223 IOA can be calculated as,

$$224 \quad IOA = 1 - \frac{\sum_i^N (O_i - S_i)^2}{\sum_i^N (|O_i - \bar{O}| + |S_i - \bar{S}|)^2} \quad (2)$$

225 where O_i and S_i denote time-dependent observations and predictions at time and location i ,
 226 respectively, N is the number of samples (by time and/or location), \bar{O} denotes mean observation
 227 and \bar{S} denotes mean predictions over all time and locations, they can be calculated as:

228
$$\bar{O} = (1/N) \sum_{i=1}^N O_i, \bar{S} = (1/N) \sum_{i=1}^N S_i,$$

229 IOA values range from 0-1, with a value of 1 indicating a perfect agreement.

230 For surface networks with hourly data, e.g., National Climatic Data Center (NCDC), the
231 observational data are paired up with the simulated data on an hourly basis for each site. The
232 observational data and simulated data are averaged out for each site. The statistics are then
233 calculated based on the site-specific data pairs. The satellite-derived data are usually available on
234 a monthly basis, and the simulated data are also averaged out on a monthly basis. The satellite-
235 derived data are regridded to the same domain and number of grid cells similar to the simulated
236 data. The time dimension is removed for the climatological evaluation, the statistics are based on
237 a site-specific average or a grid cell average. The statistics are then calculated based on the paired
238 satellite-derived vs. simulated grid cell values. The spatial and temporal analyses include spatial
239 plots of MB over CONUS, spatial overlay plots of averaged simulated and observational data,
240 monthly climatologically-averaged time series of major meteorological and chemical variables,
241 annual average time series; probability density functions of major meteorological and chemical
242 variables, and spatial plots of major aerosol and cloud variables compared with satellite data. A
243 summary of the observational data from surface networks and satellite retrievals can be found in
244 Table S3. The variables that are analyzed in this study include O₃, particulate matter with diameter
245 less than and equal to 2.5 and 10 μm (PM_{2.5} and PM₁₀, respectively), and PM_{2.5} species including
246 sulfate (SO₄²⁻), ammonium (NH₄⁺), nitrate (NO₃⁻), EC, OC, and total carbon (TC = EC + OC),
247 temperature at 2-m (T2), relative humidity at 2-m (RH2), and wind speed at 10-m (WS10), wind
248 direction at 10-m (WD10), precipitation, aerosol optical depth (AOD), cloud fraction (CLDFRA),
249 cloud water path (CWP), cloud optical thickness (COT), CDNC, cloud condensation nuclei
250 (CCN), downward shortwave radiation (SWDOWN), net shortwave radiation (GSW), downward

251 longwave radiation (GLW), outgoing longwave radiation at the top of atmosphere (OLR), and
252 shortwave and longwave cloud forcing (SWCF and LWCF). While uncertainties exist in all the
253 observational data used, systematic uncertainty analysis/quantification is beyond the scope of this
254 work. In this work, all observational data are considered to be the true values in calculating the
255 performance statistics. The information on the accuracy of most data used in the model evaluation
256 has been provided in Table 2 of Zhang et al. (2012a). Uncertainties associated with some of the
257 observational data are discussed in Section 3.

258 **3. Model Performance Evaluation**

259 **3.1 Meteorological Predictions**

260 Table 2 summarizes the statistics for T2, RH2, WS10, WD10, and precipitation. The model
261 performs very well for a 10-year average T2 with a slight underprediction (an MB of -0.3 °C).
262 This is better or consistent with other studies which tend to report underpredictions in simulated
263 T2. Brunner et al. (2014) reported a range of monthly MBs for T2 of -2 to 1 °C for simulations
264 using a number of CTMs over individual years for 2006 and 2010 with reanalysis meteorological
265 ICs/BCs. Seasonal temperature biases of -1.8 to -2.3 °C were reported from an ensemble of
266 regional climate models (RCMs) for a simulation period of 1971 to 2000 over northeastern U.S.
267 (Rawlins et al., 2012). He et al. (2015) also showed biases of -3 to 0 °C over CONUS when
268 compared against NCEP reanalysis data. Kim et al. (2013) compared the results of a number of
269 RCMs over CONUS over a climatological period of 1980 to 2003 against Climatic Research Unit
270 (CRU) surface analysis data at a 0.5° resolution and reported T2 biases of -5 to 5 °C. Figure 9.2
271 from Flato et al. (2013) shows that the Coupled Model Intercomparison Project Phase 5 (CMIP5)
272 models tend to underpredict T2 for the period of 1980 to 2005 over western U.S. by up to -3 °C.
273 The slight bias in T2 can be attributed to errors in soil temperature and soil moisture (Pleim and

274 Gilliam, 2009) or errors in the green vegetation fraction in the National Center for Environmental
275 Prediction, Oregon State University, Air Force and Hydrologic Research Lab (NOAH) Land
276 Surface Model (LSM) (Refslund et al., 2013). RH2 and WS10 are slightly overpredicted.
277 Precipitation is largely overpredicted, consistent with overpredictions in precipitation from WRF
278 and WRF/Chem simulations reported in literatures. For example, Caldwell et al. (2009) attributed
279 the overprediction in precipitation to overprediction in precipitation intensity but underprediction
280 in precipitation frequency. Otte et al. (2012) also reported that the precipitation predicted by WRF
281 is too high compared to the North American Regional Reanalyses (NARR) data throughout the
282 whole CONUS domain over a period of 1988 – 2007. Nudging and reinitialization have been most
283 commonly used methods to control such errors. . Three sensitivity simulations are conducted for
284 a summer month (July 2005) to pinpoint likely causes of the precipitation biases. The baseline
285 simulation (**Base**) uses a monthly reinitialization frequency, CESM_NCSU ICs/BCs, and the Grell
286 3D cumulus parameterization. The sensitivity simulations include (1) **Sen1**, which is similar to the
287 Base case except with a 5-day reinitialization period; (2) **Sen2**, which is similar to Base except
288 using NCEP for the meteorological ICs/BCs; and (3) **Sen3**, which is similar to Base except using
289 WRF/Chem v3.7 with the Multi-Scale Kain Fritsch (MSKF) cumulus parameterization, instead
290 of Grell 3D. The differences in configuration setup in those sensitivity simulations are given in
291 Table S4. The evaluation and comparison of the baseline and sensitivity results in July 2005 are
292 summarized in Tables S5 and S6, and Figure S1 in the supplementary material. As shown in Tables
293 S5-S6 and Figure S1, the precipitation bias can be attributed to several factors including the use of
294 Grell 3D cumulus parameterization scheme, the use of bias-corrected CESM_NCSU data (instead
295 of NCEP reanalysis data), and the use of an reinitialization frequency of 1-month, among which
296 the first factor dominates the biases in precipitation predictions. The simulated precipitation is

297 very sensitivity to different cumulus parameterizations. Compared to scale-aware
298 parameterizations such as the multi-scale Kain-Fritsch (MSKF) cumulus scheme, the Grell 3D
299 parameterization has a tendency to overpredict precipitation, particularly over ocean.

300 Figure 1 shows the spatial distributions of MB for 10-year average predictions of T2, RH2,
301 WS10, and precipitation. Figure 2 shows the time series of 10-year average monthly and annual
302 average T2, WS10, RH2, precipitation, O₃, and PM_{2.5} against observational data and IOA statistics.
303 T2 (Figure 1a) tends to be underpredicted over eastern and western U.S. and overpredicted over
304 the central U.S. The bias correction method itself may also contribute to the slight biases in T2. A
305 single temporally averaged (2001 – 2010) NCEP reanalysis file is applied to the 6-hourly BCs for
306 each individual year, which would in some cases contribute to the biases in the climatological 10-
307 year evaluation. T2 also tends to be overpredicted during the cooler months but underpredicted
308 during the warmer months (Figure 2a). While the bar charts in Figure 2 show domain- average
309 mean observed and mean simulated T2, IOA performance takes into account the proportion of
310 differences between mean observed and mean simulated values at different sites.

311 The model performance in terms of IOA for T2 is slightly worse during the warmer months
312 as compared to the cooler months; however, IOA values for all months are ≥ 0.9 . The poorer IOA
313 statistics for the warmer months are possibly influenced to a certain extent by the fact that the IOA
314 tends to be more sensitive towards extreme values (when temperatures are maximum) due to the
315 squared differences used in calculating IOA (Legates and McCabe, 1999). As shown in Figures 1b
316 and 2b, the spatial distributions of MBs for RH2 follow closely the spatial distributions of MBs
317 for T2, where T2 is underpredicted, RH2 is overpredicted and vice versa. Unlike T2, the IOA for
318 RH2 is the highest during the warmer months and the lowest during the winter months, but IOA
319 for RH2 is generally high (> 0.7) for all months. WS10 is also generally overpredicted along the

320 coast, over eastern U.S. and some portions over the western U.S. (Figure 1c), consistent with
321 overpredictions of T2 over the coast, and partially due to unresolved topographical features. In this
322 case the topographic correction for surface winds used to represent extra drag from sub-grid
323 topography (Jimenez and Dudhia, 2012) is used as an option in the 10-yr WRF/Chem simulations;
324 however, WS10 is still overpredicted except for the areas of flat undulating land in the central U.S.
325 Jimenez and Dudhia (2012) also suggested that the grid points nearest to the observational data
326 might not be the most appropriate or most representative, and that the selection of nearby grid
327 points can help to reduce errors in surface wind speed estimations. In this study, as the evaluation
328 is conducted over the whole CONUS, the nearest grid points are used for evaluation, which could
329 also result in errors in wind speed evaluation. The positive T2 and WS10 bias along the coast could
330 be due to the fact that the model grids for temperatures and wind speeds are located over the ocean,
331 however, the observation points are located slightly inland. As shown in Figure 2, WS10 performs
332 well on average for the months of April, May, and June, and is overpredicted for the other months.
333 Nonetheless the climatological NMB for WS10 overall is low at 7.7% (Table 2). WS10 has higher
334 IOA values during the spring months and the lowest IOA during the summer months and in
335 November. The model performs relatively well in predicting WD10 variability with a Corr of 0.6,
336 indicating overall a more southerly direction domain-wide predicted by the model compared to
337 observations. Precipitation is overpredicted for all months except for June, especially during the
338 summer months of July to August. Even with the inclusion of radiative feedback effects from the
339 subgrid-scale clouds in the radiation calculations, precipitation is still overpredicted with the Grell
340 3D scheme, which is consistent with the results shown by Alapaty et al. (2012). Precipitation
341 mainly has lower IOAs during the summer compared to other months, except in June which
342 actually exhibits the largest IOA of all months. Even though June is considered a summer month,

343 it does not show overprediction in precipitation compared to the other summer months. It is
344 possible that in June, the overall atmospheric moisture content is low. This is consistent with
345 simulated RH2 as June is the only month where RH2 is underpredicted compared to observations.

346 In general the model is able to reproduce the monthly trends in meteorological variables;
347 for example, the predicted trend in T2 closely follows the observed trends by NCDC. The observed
348 RH2 decreases from January to a minimum in April, and then increases from April to December.
349 Although the model predicts a similar pattern in RH2, there is a lag in the RH2 minimum occurring
350 two months later in June (Figure 2b). For WS10, the observation peaks in April, as compared to
351 the simulated peak in March. The model correctly predicts the observed WS10 minimum occurring
352 in August. The model trend in precipitation is similar to observations, except during the summer
353 months of July through September, where a large overprediction leads to a sharp increase in July,
354 followed by a gradual decrease through December.

355 Figures 2e – 2h show the annual time series trends for T2, RH2, WS10, and precipitation.
356 The model performs relatively well in predicting the annual mean T2 for most years (with MBs of
357 < 0.5 °C; Figure 2e). T2 also does not show an obvious decreasing or increasing T2 trend between
358 2001 and 2010. The IOA for annual T2 for all years are > 0.95 . However for 2002, mean simulated
359 T2 is ~ 0.7 °C higher than the observational data. IOA is still high for 2002 which indicates
360 probably good performance of T2 at most sites, however with large overpredictions at a few sites
361 which could skew the mean observed and mean simulated value but not influence IOA
362 significantly. RH2 is consistently overpredicted by the model with the largest overprediction in
363 2009. With the exception of 2009, observed RH2 is rather steady (65 – 70 %) from 2001 to 2010.
364 IOA is also steady for RH2, except for 2009. As mentioned earlier, WRF tends to overpredict
365 WS10 in general. Figure 2g shows that observations indicate weaker wind speeds from 2001 to

366 2007. Model performance is better from 2007 to 2010 with higher IOAs compared to previous
367 years. WRF has worse performance especially at weaker wind speeds as is the case from 2001 to
368 2007. Model performance for precipitation is more variable year-to-year, with IOAs ranging from
369 0.4 to 0.7; however, there is a systematic positive bias during the 10 year period.

370 Figure 3 shows the probability density functions (PDFs) of T2, RH2, WS10, and
371 precipitation against NCDC and NADP for 10 years. The observed and simulated variables are
372 averaged at each site for the 10-year period, and the pairs are then distributed into a PDF over 30
373 bins of observed and simulated values of T2. For T2, the simulated and observed PDFs are very
374 similar (Figure 3a), consistent with the statistics for T2 which shows only a small cold bias. The
375 model overpredicts T2 at sites where temperatures are very low. The PDF for simulated RH2 is
376 also shifted to the right of the observed RH2 (Figure 3b), with an observed and modeled peak 74%
377 and 78% respectively. The PDF of simulated WS10 is narrower (between 2 and 6 m s⁻¹) compared
378 to that of observed WS10 (between 1 and 7 m s⁻¹). The model thus overpredicts when near-surface
379 wind speeds are low, but underpredicts when wind speeds are very high. This suggests that the
380 surface drag parameterization is still insufficient to help predict low wind speeds; however, it
381 might have contributed to the reduction in the simulated high wind speeds (Mass, 2012). The PDF
382 for simulated precipitation against NADP also shows a shift to the right, consistent with the
383 statistics for overpredicted precipitation and also with the PDF of RH2. Nasrollahi et al. (2012)
384 examined 20 combinations of microphysics and cumulus parameterization schemes available in
385 WRF and found that most parameterization schemes overestimate the amount of rainfall and the
386 extent of high rainfall values. In this study, while Grell 3D Ensemble cumulus parameterization
387 contributes in part to the overpredictions of precipitation, most overpredictions occur at high
388 thresholds as shown in Figure 3 (d) and they are attributed to possible errors in the Morrison two

389 moment scheme because the overpredictions of non-convective precipitation dominate the
390 overpredictions of total precipitation.

391 **3.2 Chemical Predictions**

392 **3.2.1 Ozone**

393 Table 2 summarizes the statistics for major chemical species. The model overpredicts
394 hourly O₃ mixing ratios on average against the Aerometric Information Retrieval System (AIRS)
395 – Air Quality System (AQS) with an NMB of 9.7% and an NME of 22.4%, but underpredicts O₃
396 mixing ratios against the Clean Air Status and Trends Network (CASTNET) with an NMB of -
397 8.8% and an NME of 19.8%. The O₃ mixing ratios are overpredicted at AIRS-AQS sites for all
398 climatological months except for April and May (Figure 4a) but underpredicted at CASTNET sites
399 for all months except for October with the largest underpredictions occurring in April and May
400 where IOA statistics are the lowest (Figure 4b). IOA statistics for all climatological months range
401 from 0.5 to 0.6 for AIRS-AQS and from 0.4 to 0.9 for CASTNET. In general, IOA values tend to
402 be higher for CASTNET compared to AIRS-AQS during the fall and winter months of October to
403 March. The IOA values for AIRS-AQS are rather steady on average over the 12 months compared
404 to CASTNET. This can be attributed to the larger dataset of AIRS-AQS (> 1000 stations)
405 compared to CASTNET (< 100 stations), the high and low undulations in O₃ averages at the
406 CASTNET sites tend to be smoothed or averaged out in O₃ averages at the AIRS-AQS sites given
407 larger AIRS-AQS dataset. The observed data from AIRS-AQS and CASTNET also show the
408 highest monthly O₃ mixing ratios over April and May. This result is consistent with the findings
409 of Cooper et al. (2014), who reported the highest mass of tropospheric O₃ for the northern
410 hemisphere in April and May based on the Ozone Monitoring Instrument (OMI) measurements in
411 2004, which suggested that the column mass of O₃ is not necessarily proportional to nitrogen oxide

412 (NO_x) emissions that peak during the summer. In addition, Cooper et al. (2014) attributed a shift
413 in the seasonal O₃ cycle observed at many rural mid-latitude monitoring sites to emissions
414 reductions in the U.S. The same study also reported that the summertime O₃ mixing ratios were
415 lower in eastern U.S. between 2005 and 2010 when compared to previous years, while remaining
416 relatively constant in spring. Thus the summer O₃ maximum during 2001- 2004 was replaced by
417 a broad spring/summer peak in 2005 - 2010. Both the observed and simulated O₃ mixing ratios do
418 not decrease for AIRS-AQS and CASTNET from 2001 to 2010 (Figures 4e and 4f). This is
419 somewhat consistent with Cooper et al. (2014) which showed that surface and lower tropospheric
420 O₃ has a decreasing trend over eastern U.S. but an increasing trend over the western U.S. from
421 1990-1999 to 2010. The predicted annual average O₃ mixing ratios are consistent from 2001 to
422 2010, with overpredictions and IOAs of ~0.6 at the AIRS-AQS sites, and underpredictions and
423 IOAs of ~0.6 to 0.8 at the CASTNET sites.

424 Figure 5 shows the PDFs of maximum 1-hour and 8-hour O₃ mixing ratios against
425 CASTNET and AIRS-AQS. The PDF of the observed and simulated O₃ mixing ratios are very
426 similar. The model is able to simulate the range and probabilities of O₃ mixing ratios relatively
427 well at both CASTNET and AIRS-AQS sites. At the CASTNET sites as shown in Figures 5a and
428 b, the model accurately predicts the peak maximum 1-hour O₃ mixing ratio centered at ~60 ppb,
429 however, slightly underpredicts the peak maximum 8-hour O₃ mixing ratio by a few ppb. At the
430 AIRS-AQS sites as shown in Figures 5c and d, the predicted PDF is slightly shifted to the right of
431 the observations for both maximum 1-hour and 8-hour O₃ mixing ratios. It is also interesting to
432 note that the PDFs for CASTNET and AIRS-AQS are quite different. O₃ at the AIRS-AQS sites
433 has a unimodal normal distribution, while O₃ at the CASTNET sites has a bi-modal distribution,
434 with a tail of the distribution extending toward lower O₃ mixing ratios (0 – 20 ppb). The peak

435 distribution occurs at around 10 ppb, because the O₃ mixing ratios are low at most CASTNET
436 sites. The second peak at ~60 ppb for CASTNET occurs mainly around the summer months during
437 which O₃ is produced through photochemistry involving its precursors. These distributions are
438 attributed to the nature of the sites' locations, where the AIRS-AQS network includes a mixture
439 of urban, suburban and rural sites, leading to a normal distribution of O₃ mixing ratios centered at
440 relatively higher O₃ mixing ratios, while the CASTNET network includes mostly rural sites that
441 exhibit a low maximum 1-hour and 8-hour O₃ mixing ratios, thus leading to a distribution with a
442 tail skewed towards the lower O₃ mixing ratios.

443 Figure 6 shows the diurnal variation of O₃ concentrations and IOA statistics for the four
444 climatological seasons against CASTNET (Figures a to d) and AIRS-AQS (Figures e to h) (Winter
445 - January, February and December (JFD); Spring - March, April, and May (MAM); Summer -
446 June, July, and August (JJA); Fall - September, October, and November (SON). Figure 6a shows
447 that in more rural sites (CASTNET) in winter O₃ tends to be underpredicted during the morning
448 (01:00 – 09:00 local standard time (LST)) and evening hours (18:00 – 24:00 LST). However,
449 Figure 6b shows that in general for all AIRS-AQS sites including urban sites, O₃ is systematically
450 overpredicted for all hours of the day. The diurnal trends for CASTNET and AIRS-AQS are
451 completely opposite for winter. As CASTNET sites are located in areas where urban influences
452 are minimal, most of these sites are likely to be NO_x-limited sites (Campbell et al., 2014).
453 Underpredicted NO_x emissions in rural areas can lead to underpredictions in O₃ concentrations in
454 NO_x-limited areas. As shown in Figure 2a), T2 is generally overpredicted during the winter
455 months, which explains the overpredictions in O₃ for most sites against AIRS-AQS. As shown in
456 Figures 6a, b and c, for CASTNET, the diurnal variations of O₃ in MAM and JJA are similar to
457 that in JFD. As shown in Figure 6d, slight overpredictions during the daylight hours of 10:00 to

458 17:00 LST occur in SON at the CASTNET sites, however the trends are similar for morning and
459 evening hours as compared to the other seasons. Similar to SON at the CASTNET sites, for AIRS-
460 AQS sites, overpredictions during daylight hours occur in JJA and SON (Figures 6 g and h), and
461 also to a much lesser extent in MAM (Figure 6f). This is probably due to the overpredictions of
462 T2, which are the smallest during MAM compared to other months as shown in Figure 2a.

463 Figure 7 compares the spatial distributions of 10-year average of the predicted and
464 observed hourly O₃ mixing ratios. The O₃ mixing ratios tend to be underpredicted in eastern and
465 northeastern U.S., where most of the CASTNET sites are located (Figure 7a). This is consistent
466 with the diurnal trends from Figures 6a to d which also show underpredictions for CASTNET sites.
467 From Figure 1a, T2 is underpredicted on average over northeastern U.S., which results in
468 underpredictions in biogenic emissions in the rural areas from MEGAN2. This would in turn
469 reduce O₃ mixing ratios in VOC-limited areas. O₃ photochemical reactivities would also be
470 reduced due to reduced T2. O₃ mixing ratios are, however, overpredicted over northwestern U.S.,
471 and also near the coastline of western U.S. The overprediction of O₃ mixing ratios in northwestern
472 U.S. can be attributed to an overprediction in the chemical BCs from CESM, as indicated by the
473 high O₃ mixing ratios near the northwestern region of the domain boundary.

474 **3.2.2 Particulate Matter**

475 The 10-year average PM_{2.5} concentrations are overpredicted with an NMB of 23.3 %
476 against IMPROVE, and underpredicted with an NMB of -10.8 % against the Speciated Trends
477 Network (STN) (Table 2). In addition, the IOA trend in Figure 4c shows very good performance
478 for PM_{2.5} against the Interagency Monitoring of Protected Visual Environments (IMPROVE) with
479 IOA values > 0.8. IOA values for PM_{2.5} against STN are high (~ 0.6 – 0.8) during the spring and
480 summer months, but lower (~ 0.4) during the winter months (Figure 4d). The IMPROVE surface

481 network covers generally rural areas and national parks while the STN surface network covers
482 urban sites. The horizontal resolution of $36 \times 36 \text{ km}^2$ used in this study may be too coarse to resolve
483 the locally high $\text{PM}_{2.5}$ concentrations at urban sites in STN which are in proximity of significant
484 point sources, especially during the fall and winter. During these colder seasons, $\text{PM}_{2.5}$
485 concentrations over the U.S. in general tend to be higher due to an extensive use of woodstove and
486 cold temperature inversions, which trap particulates near the ground (EPA, 2011). As shown in
487 Table 2, the concentrations of $\text{PM}_{2.5}$ species such as SO_4^{2-} , OC, and TC are overpredicted at the
488 IMPROVE sites, while the concentrations of the other main $\text{PM}_{2.5}$ species NO_3^- , NH_4^+ , and EC are
489 underpredicted at both IMPROVE and STN sites. TC concentrations, which are the sum of OC
490 and EC, are overpredicted due to larger overpredictions of OC compared to the underpredictions
491 of EC. The model also simulates both primary organic aerosol (POA) and secondary organic
492 aerosol (SOA). OC is calculated as the sum of POA and SOA divided by the ratio of OA/OC,
493 which is assumed to be a constant of 1.4 (Aitken et al., 2008). This calculation of OC using a
494 constant of 1.4 is an approximation, which is subject to uncertainties when comparing simulated
495 OC against observational data, as the ratio of OA/OC can be different in different environments
496 (Aitken et al., 2008).

497 As shown in Table 2, at the STN sites, the model slightly overpredicts the concentrations
498 of SO_4^{2-} , while underpredicting those of NO_3^- , NH_4^+ , and EC. The overpredictions of SO_4^{2-} are
499 likely due to the uncertainties that arise from processing of the RCP SO_2 emissions. The RCP SO_2
500 emissions are only available as a total emission flux, and they are not vertically distributed to the
501 important point sources such as furnaces and stacks. In this work, two steps are taken to resolve
502 the RCP elevated SO_2 emissions in each emission layer. First, a set of factors are derived from the
503 fraction of the elevated emissions in each layer to the vertical sum of emissions for NEI used by

504 default in the SMOKE model with the NEI data. Second, these factors are applied to the total RCP
505 emissions to obtain SO₂ emissions in each emission layer. The total RCP SO₂ emissions were
506 higher than the total NEI emissions, resulting in higher surface and elevated SO₂ emissions.
507 Figures 4g and 4h compare the modeled annual average time series for PM_{2.5} against IMPROVE
508 and STN observations, respectively. In general, the model performs well for PM_{2.5} at the
509 IMPROVE (IOA > 0.8) and STN (IOA ~ 0.5 – 0.7) sites. A declining trend in PM_{2.5} observed and
510 simulated concentrations are also observed over the years. For the later years (2007 to 2010), the
511 model performs significantly better against IMPROVE compared to STN. As 2010 NEI emissions
512 are used for the years 2007 to 2010, there are not many variations in the simulated PM_{2.5}
513 concentrations over these 4 years.

514 Figures 7 and 8 show the spatial plots of 10-yr average of simulated 24-hour average ,
515 PM₁₀, PM_{2.5}, and PM_{2.5} species concentrations, overlaid with observations from both STN and
516 IMPROVE. The underpredictions of PM₁₀ are dominated by an underprediction in the wind-blown
517 dust emissions, especially in western U.S. (Figure 7b). This is confirmed in Table 2, which shows
518 an MB of -11.5 μg m⁻³ and an NMB of -51.2% against PM₁₀ observations at AIRS-AQS sites. The
519 observational data indicate the elevated concentrations of dust over portions of Arizona and
520 California (> 50 μg m⁻³), which are not reproduced by the simulations (the simulated
521 concentrations are much lower, < 20 μg m⁻³). The AER/AFWA dust module (Table 1) does not
522 produce sufficient dust in this case, even though WS10 is overpredicted and is proportional to the
523 dust emissions. The sea-salt emission module by Gong et al. (1997), however, seems to produce a
524 reasonable amount of sea-salt as shown by the similar concentrations between simulated and
525 observational data for PM₁₀ near the coastlines. In addition, the MADE/VBS module in
526 WRF/Chem does not explicitly simulate the formation/volatilization of coarse inorganic species.

527 The coarse inorganic species are available, however, in the emissions and are transported and
528 deposited in a manner that is similar to non-reactive tracers.

529 The model performs well for $PM_{2.5}$ over eastern U.S. (Figure 7c), where modeled
530 concentrations are close to the observations; however, over the western U.S. there are
531 underpredictions in $PM_{2.5}$, especially in central to southern California. Even though Table 2 shows
532 in general an overprediction of SO_4^{2-} against STN sites, the model underpredicts SO_4^{2-} in regions
533 of elevated SO_4^{2-} concentrations, in particular, where concentrations are above $10 \mu\text{g m}^{-3}$ in the
534 vicinity of significant point sources of SO_2 and SO_4^{2-} over eastern U.S. (Figure 7d). This is likely
535 due to the coarse resolution ($0.5^\circ \times 0.5^\circ$) of RCP emissions, which probably results in a general
536 overprediction of SO_2 emissions over a grid but cannot resolve point sources smaller than the grid
537 resolution. A similar pattern is found for NH_4^+ over eastern U.S. due to underpredictions of high
538 concentrations of SO_4^{2-} (Figure 8a). There are also large underpredictions in NH_4^+ over the western
539 U.S. The underpredictions in NH_4^+ are likely due to underpredictions of NH_3 emissions from RCP.
540 The NH_3 emissions from RCP are much lower than those of NEI emissions over western U.S., by
541 more than a factor of 5, especially over portions of California. Large underpredictions occur over
542 both eastern and western U.S. for NO_3^- , EC, and TC (Figures 8b, c, and d). The underpredictions
543 in NO_3^- are more likely influenced by the underpredictions of NH_4^+ rather than NO_x emissions.
544 NO_x emissions for NEI are higher than those of RCP for a number of point sources, however, in
545 general RCP has higher NO_x emissions. Other possible reasons for the underpredictions of NO_3^-
546 concentrations include both prediction and measurement errors associated with SO_4^{2-} and TNH_4
547 that can greatly affect the performance of NO_3^- , inaccuracies in the assumptions used in the
548 thermodynamic model (e.g., the assumption that inorganic ions are internally mixed and the
549 equilibrium assumption might not be representative, especially for particles with larger diameters),

550 as well as inaccuracies in T2 and RH predictions (Yu et al., 2005). The statistics for IMPROVE
551 TC indicate overpredictions; however the statistics for STN TC indicate larger underpredictions
552 with an MB of $-2.0 \mu\text{g m}^{-3}$, which would explain the large underpredictions in $\text{PM}_{2.5}$ concentrations
553 over western U.S. The large underpredictions are in part impacted by uncertainties in emissions as
554 well as due to uncertainties in the precursor gas emissions for these species, especially for TC. The
555 RCP emissions of EC and POA are lower when compared to those of NEI. NEI emissions have a
556 higher spatial resolution, and thus more adequately represent the emissions from point sources
557 compared to RCP. The underpredictions of TC are also more likely due to underpredictions in EC
558 as compared to OC, as shown in underpredictions of EC by Figure 8c. As T2 is slightly
559 underpredicted, these could have resulted in underpredictions in isoprene and terpene, which are
560 major gas precursors of biogenic SOA, resulting in lower SOA and OC concentrations. In addition,
561 the emissions of anthropogenic VOC species from RCP which are also of a lower spatial resolution
562 compared to their emissions in the NEI tend to also be lower than NEI levels especially at point
563 sources. The underpredictions for these particulate species, especially for water-soluble species
564 including NH_4^+ and NO_3^- are also likely impacted by overpredictions in precipitation (Figure 2d),
565 which leads to an overprediction in their wet deposition rates and thus a reduction of their ambient
566 concentrations. The overpredictions in WS10 also help contribute to the deposition of $\text{PM}_{2.5}$ and
567 $\text{PM}_{2.5}$ species onto the ground (Sievering et al., 1987).

568 **3.3 Aerosol, Cloud, and Radiation Predictions**

569 There are uncertainties in the satellite retrievals of various aerosol-cloud-radiation
570 variables from the Clouds and the Earth's Radiant Energy System (CERES) and the Moderate
571 Resolution Imaging Spectroradiometer (MODIS). Loeb et al. (2009) reported that the major
572 uncertainties of the top of atmosphere radiative fluxes from CERES are derived from instrument

573 calibration (with a net error of 4.2 W m^{-2}), and the assumed value of 1 W m^{-2} for total solar
574 irradiance. However, there is good correlation ($R > 0.8$) between the model and CERES for the
575 radiation variables SWDOWN, GSW, and GLW, which are all measured at the surface (Table 2).
576 Modeled OLR at the top of the atmosphere also has relatively good correlation ($R \sim 0.6$).
577 SWDOWN and GLW are both slightly overpredicted due to influences from biases in PM
578 concentrations and clouds, but GSW and OLR are slightly underpredicted.

579 The overpredictions of the surface radiation variables are also impacted by the
580 underpredictions in AOD and COT. AOD is underpredicted with an NMB of -24.0%, and COT is
581 underpredicted with an NMB of -44.3%. These underpredictions indicate that less radiation is
582 attenuated (i.e., absorbed or scattered) or reflected while traversing through the atmospheric
583 column and clouds, thus allowing more radiation to reach the ground. Using the CESM model, He
584 et al. (2015) also showed underpredictions in AOD and COT over CONUS against MODIS
585 satellite retrievals. Figure 9 compares the spatial distributions of the 10-year average predictions
586 of AOD (a and b) against the satellite retrieval data from MODIS. The simulated AODs show
587 relatively large values over eastern U.S., due to the relatively higher PM concentrations in this
588 region of the U.S. The MODIS AOD, however, shows slightly elevated values over eastern U.S.,
589 but the magnitudes are not as high as the simulated AOD over eastern U.S. MODIS-derived AOD
590 is also higher over western U.S. compared to eastern U.S., and this trend is not found in the
591 simulated AOD. The differences between the MODIS AOD and the simulated AOD are likely due
592 to the differences in the algorithms used to retrieve AOD based on MODIS measurements and
593 calculate AOD in WRF/Chem. For MODIS, AOD is calculated by matching the spectral
594 reflectance observations with a lookup table based on a set of aerosol parameters including the
595 aerosol size distributions from a variety of aerosol models, which differ based on seasons and

596 locations (Levy et al., 2007). There are also different algorithms for dark land, bright land, and
597 over oceans (Levy et al., 2013). The MODIS data are aggregated into a global 1° gridded (Level-
598 3) dataset with monthly (MOD08_M3) temporal resolution
599 ([https://www.earthsystemcog.org/site_media/projects/obs4mips/TechNote MODIS L3 C5 Aer](https://www.earthsystemcog.org/site_media/projects/obs4mips/TechNote_MODIS_L3_C5_Aer)
600 [osols.pdf](#)). The inaccuracies for the calculation of AOD in WRF/Chem include biases in aerosol
601 size distribution, aerosol composition, aerosol water content, and reflectances. They can also arise
602 from parameterizations in the calculations including the assumption of an internally-mixed aerosol
603 composition. Therefore, caution should also be taken when comparing simulated AOD with the
604 satellite-derived AOD products. Toth et al. (2013) compared Aqua MODIS AOD products over
605 the mid to high latitude Southern Ocean where a band of enhanced AOD is observed, to cloud and
606 aerosol products produced by the Cloud-Aerosol Lidar with Orthogonal Polarization (CALIOP)
607 project; and AOD data from the Aerosol Robotic Network (AERONET) and the Maritime Aerosol
608 Network (MAN). They concluded that the band of enhanced AOD is not detected in the CALIOP,
609 AERONET, or MAN products. The enhanced AOD band is attributed to stratocumulus and low
610 broken cumulus cloud contamination, as well as the misidentification of relatively warm cloud
611 tops compared with surrounding open seas.

612 Figure 9 also shows spatial distributions of the 10-year average predictions of CDNC (c
613 and d), CWP (e and f), and COT (g and h), compared against the satellite retrieval data from
614 MODIS. The cloud variables CDNC, CWP, and COT tend to be underpredicted for most of the
615 regions over the U.S. However, CWP is largely overpredicted over the Atlantic ocean. This is also
616 likely due to the build-up of moisture over the Atlantic ocean, also influencing precipitation as
617 mentioned previously. CDNC is overpredicted over some regions in eastern U.S., but there are
618 also relatively large areas of underpredictions over both the land and ocean. This leads to an

619 average domain-wide underprediction for CDNC (Table 2). This is likely due to the differences in
620 deriving CDNC in the model and in the satellite retrievals. CDNC in the model is calculated based
621 on the activation parameterization by Abdul Razzak and Ghan (2000) based on the aerosol size
622 distribution, aerosol composition, and the updraft velocity. The MODIS-derived CDNC from
623 Bennartz (2007) is calculated based on cloud effective radius and COT, which would explain the
624 differences in spatial patterns between model and observed data. As indicated by Bennartz (2007),
625 the errors in CDNC can be up to 260%, especially for regions with low CF (< 0.1). The model and
626 MODIS spatial patterns are similar for CWP and COT over land, although the model values are
627 underpredicted. King et al. (2013) reported that the MODIS retrieval of cloud effective radius
628 when compared to in-situ observations is overestimated by 13% on average. Combined with
629 overestimations in COT, this leads to overestimation of liquid water path. In addition, there can
630 also be differences in satellite-derived cloud products from different satellites. For example, Shan
631 et al. (2011) showed that the derived CLDFRA from MODIS and another satellite, the Polarization
632 and Directionality of Earth Reflectances (POLDER) can differ with a global average of 10%.

633 Figure 10 shows similar spatial plots for modeled versus CERES derived SWDOWN,
634 OLR, SWCF, and LWCF. We note that modeled SWCF is calculated based on the differences
635 between the net cloudy sky and net clear sky shortwave radiation at the top of atmosphere, which
636 in turn are dependent on cloud properties including the CLDFRA, COT, cloud asymmetry
637 parameter, and cloud albedo. It is possible that due to the overprediction of CLDFRA, the
638 magnitudes of the simulated SWCF are greater than those from CERES (Figures 10c and 10g),
639 even though the other cloud variables are underpredicted. LWCF is calculated based on the
640 differences in clear-sky OLR and cloudy-sky OLR, which in turn are dependent on CLDFRA,
641 COT, and absorbance and radiance due to atmospheric gases. The underprediction of total-sky

642 OLR (Table 2 and Figures 10b and 10f) leads to an overprediction in LWCF. SWCF is largely
643 overpredicted over eastern U.S. and especially over the Atlantic ocean (Figures 10c and 10g).
644 LWCF is also overpredicted by the model in similar locations as SWCF, such as in southeastern
645 U.S., and over the ocean in the eastern portion of the domain (Figures 10d and 10h). This is further
646 confirmed by the underpredictions in SWDOWN over the Atlantic ocean and in general over the
647 eastern portion of the domain, as increased clouds (as a consequence of overpredicted AOD, CWP
648 and COT) and SWCF lead to less SWDOWN reaching the ground (Figures 10a and 10e) which
649 also eventually leads to a reduction in the OLR also over the eastern portion of the domain. The
650 larger negative SWCF and positive LWCF in the model compared to CERES, however, lead to an
651 overall good agreement with CERES for the net cloud forcing (SWCF + LWCF; not shown). The
652 mean bias for SWCF against CERES of 7.8 W m^{-2} and that for LWCF against CERES of 6.9 W
653 m^{-2} are comparable to the results from the CMIP5 models of -10 to 10 W m^{-2} over CONUS region
654 (Figure 9.5 in Flato et al., 2013). The evaluation of 10-year averaged predictions of aerosol-cloud-
655 radiation variables is similar to the results from the WRF/Chem simulations in 2006 and 2010 by
656 Yahya et al. (2014 and 2015). For example WRF/Chem generally performs well for cloud fraction
657 but AOD, CDNC, CWP and COT are underpredicted in both studies, which possibly indicate
658 consistent biases for every year contributing to climatological biases.

659 **4. Summary and Conclusions**

660 Overall, the model slightly underpredicts T2 with a mean bias of $\sim -0.3 \text{ }^\circ\text{C}$, which is
661 consistent or better than other studies based on chemical transport models and regional climate
662 models. The underpredictions in T2 correlate to the overpredictions in RH2. WS10 biases are
663 likely due to issues with unresolved topography or due to inaccuracies in the selection of
664 representative grid points. There are seasonal biases in precipitation, where overpredictions tend

665 to occur largely over the summer months; however, precipitation is overpredicted every year
666 between 2001 and 2010 likely due mainly to uncertainties in WRF cumulus and microphysics
667 parameterizations. In particular, the use of a different cumulus parameterization scheme, e.g.,
668 based on the MSKF available in WRF/Chem version 3.7 or newer has been shown in the sensitivity
669 study to significantly reduce precipitation biases. Other factors contributing to the precipitation
670 bias include the use of bias-corrected CESM_NCSU data (instead of NCEP reanalysis data), and
671 the use of an reinitialization frequency of 1-month. A satisfactory model performance for
672 meteorological variables is important and necessary when simulating future years, as data
673 evaluation is not possible. Meteorological variables such as temperature, humidity, wind speed
674 and direction, PBL height, and radiation have a strong impact on chemical predictions, and thus
675 are critical to the satisfactory model performance when predicting chemical variables such as O₃
676 and PM_{2.5}. Biases in O₃ and PM_{2.5} concentrations can be attributed to biases in any of the
677 meteorological and chemical variables. The model performs generally well for radiation variables,
678 as well as for the main chemical species such as O₃ and PM_{2.5}, which indicates that the processed
679 RCP 8.5 emissions are reasonably accurate to produce acceptable results for the concentrations of
680 chemical species.

681 Modeled O₃ mixing ratios at the CASTNET sites are slightly underpredicted, but are
682 slightly overpredicted at AIRS-AQS sites, in part due to the fact that the CASTNET sites are
683 classified as rural, while the AIRS-AQS sites are classified as both urban and rural. O₃ mixing
684 ratios at the AIRS-AQS sites tend to be overpredicted during the colder fall and winter seasons,
685 and annually, O₃ mixing ratios are overpredicted every year from 2001 to 2010. O₃ mixing ratios
686 at the CASTNET sites are underpredicted for all climatological months, while the largest
687 underpredictions are observed from January to May. However, on a decadal time scale,

688 WRF/Chem adequately represents the different O₃ PDFs at the AIRS-AQS and CASTNET sites.
689 This study also showed that peak O₃ mixing ratios are observed over April and May rather than
690 June to August, which is consistent with Cooper et al. (2014) who attributed this to emission
691 reductions and opposite trends in O₃ mixing ratios over eastern and western U.S. over the last 20
692 years. Modeled PM_{2.5} concentrations tend to be overpredicted at the IMPROVE sites but
693 underpredicted at the STN sites. PM_{2.5} at the IMPROVE sites tend to be underpredicted in spring
694 and summer but overpredicted in fall and winter, while PM_{2.5} concentrations against STN are
695 persistently underpredicted for all climatological months. The IMPROVE and STN sites are
696 classified as rural and urban, respectively. Due to the relatively coarse horizontal resolution of the
697 model (36 × 36 km), the model is unable to capture the locally higher PM_{2.5} concentrations at the
698 STN sites. In general, however, the model performs relatively well for total PM_{2.5} concentrations
699 at the IMPROVE and STN sites with NMBs of within ±25%, although larger biases exist for PM_{2.5}
700 species. Model performance for PM₁₀ should be improved, as PM₁₀ also has important impacts on
701 climate through influencing the radiative budget both directly and indirectly due to its larger size
702 and higher concentrations. The choice of observational networks for model evaluation are
703 therefore important as both networks can show positive and negative biases depending on the type
704 and location of the sites (e.g., O₃ against AIRS-AQS and CASTNET, and PM_{2.5} against STN and
705 IMPROVE). The major uncertainties lie in the predictions of cloud-aerosol variables. As
706 demonstrated in this study, large biases and error in simulating cloud variables even in the most
707 advanced models such as WRF/Chem, indicating a need for future improvement in relevant model
708 treatments such as cloud dynamics and thermodynamics, as well as aerosol-cloud interactions. In
709 addition, there are large uncertainties in satellite retrievals of cloud variables for evaluation. In this
710 study, most of the cloud-aerosol variables including AOD, COT, CWP, and CDNC are on average

711 underpredicted across the domain; however, the overpredictions of cloud variables including COT
712 and CWP over the Atlantic ocean and eastern U.S. lead to underpredictions in radiation and
713 overpredictions in cloud forcing, which are important parameters when simulating future climate
714 change.

715 In summary, the model is able to predict O₃ mixing ratios and PM_{2.5} concentrations
716 relatively well with regards to decadal scale air quality and climate applications. The model is able
717 to predict meteorological variables satisfactorily and with results comparable to RCM and GCM
718 applications from literatures. Possible reasons behind the chemical and meteorological biases
719 identified through this work should be taken into account when simulating longer climatological
720 periods and/or future years. Aerosol-cloud-radiation variables are important for climate
721 simulations, the performance of these variables are not as good as that of the chemical and
722 meteorological variables. They contain consistent biases in single-year evaluations of WRF/Chem.
723 However, magnitudes of biases for SWCF and LWCF are comparable to those from literature,
724 which suggests that model improvements should be made in terms of bias correction of
725 downscaled ICs/BCs as well as aerosol-cloud-radiation parameterizations in the model. In
726 addition, having consistent physical and chemical mechanisms between the GCM and RCMs could
727 help to reduce uncertainties in the results (Ma et al., 2014). Although CESM and WRF/Chem use
728 similar chemistry and aerosol treatments in this work, they use somewhat different physics
729 schemes which may contribute to such uncertainties. The development of scale-aware
730 parameterizations that can be applied at both global and regional scales would help reduce
731 uncertainties associated with the use of different schemes for global simulations and downscaled
732 regional simulations.

733

734 **Code and Data Availability**

735 The WRF/Chem v3.6.1 code used in this paper will be available upon request. However,
736 we highly encourage users to download the latest available version of the WRF/Chem code from
737 NOAA's web site at http://www2.mmm.ucar.edu/wrf/users/download/get_source.html. The
738 updates in our in-house version of WRF/Chem v3.6.1 has been implemented into WRF/Chem
739 v3.7 and WRF/Chem v3.7.1 for scientific community release. The WRF/Chem v3.7 and
740 WRF/Chem v3.7.1 codes are now publicly available at
741 http://www2.mmm.ucar.edu/wrf/users/download/get_source.html. These latest versions of the
742 source codes contain all major changes in the standard version of WRF/Chem v3.6.1 used in for
743 this study. In addition, they have been rigorously tested for compatibility and compiling issues
744 on various platforms. The inputs including the meteorological files, meteorological initial and
745 boundary conditions, chemical initial and boundary conditions, model set-up and configuration,
746 and the namelist set-up, and instructions on how to run the simulations for a 1-day test case, as
747 well as a sample output for 1-day test can be provided upon request.

748 **Acknowledgments**

749 This study is funded by the National Science Foundation EaSM program (AGS-1049200) at
750 NCSU. The emissions for chemical species that are not available from the RCP emissions are
751 taken from the 2008 NEI-derived emissions for 2006 and 2010 provided by the U.S. EPA,
752 Environment Canada, and Mexican Secretariat of the Environment and Natural Resources
753 (Secretaría de Medio Ambiente y Recursos Naturales-SEMARNAT) and National Institute of
754 Ecology (Instituto Nacional de Ecología-INE) as part of the Air Quality Model Evaluation
755 International Initiative (AQMEII). The hourly temporal profiles of 2001, 2005, and 2010 RCP
756 emissions are based on the 2002NEI and the AQMEII 2006 and 2010 emissions derived based on

757 the 2008 NEI. The authors acknowledge use of the WRF-Chem preprocessor tool mozbc provided
758 by the Atmospheric Chemistry Observations and Modeling Lab (ACOM) of NCAR and the script
759 to generate initial and boundary conditions for WRF based on CESM results provided by Ruby
760 Leung, PNNL. For WRF/Chem simulations, we would like to acknowledge high-performance
761 computing support from Yellowstone (ark:/85065/d7wd3xhc) provided by NCAR's
762 Computational and Information Systems Laboratory, sponsored by the National Science
763 Foundation.

764

765 **References**

766 Abdul-Razzak, H. and Ghan, S. J.: A parameterization of aerosol activation, 2. Multiple aerosol
767 types, *J. Geophys. Res.*, 105(5), 6837-6844, 2000.

768 Aitken, A.C., DeCarlo, P.F., Kroll, J.H., Worsnop, D.R., Huffman, J.A., Docherty, K.S., Ulbrich,
769 I.M., Mohr, C., Kimmel, J.R., Sueper, D., Sun, Y., Zhang, Q., Trimborn, A., Northway, M.,
770 Ziemann, P.J., Canagaratna, M.R., Onasch, T.B., Alfarra, M.R., Prevot, A.S.H., Dommen, J.,
771 Duplissy, J., Metzger, A., Baltensperger, U. and Jimenez, J.L.: O/C and OM/OC ratios of
772 primary, secondary and ambient organic aerosols with high-resolution time of flight aerosol
773 mass spectrometry, *Environ. Sci. Technol.*, 42, 4478 – 4485, 2008.

774 Alapaty, K., Herwehe, J., Nolte, C.G., Bullock, R.O., Otte, T.L., Mallard, M.S., Dudhia, J. and
775 Kain, J.S.: Introducing subgrid-scale cloud feedbacks to radiation in WRF, the 13th WRF Users
776 Workshop, Boulder, CO, June 26 to 29, 2012.

777 Ahmadov, R., McKeen, S.A., Robinson, A.L., Bareini, R., Middlebrook, A.M., De Gouw, J.A.,
778 Meagher, J., Hsie, E.-Y., Edgerton, E., Shaw, S. and Trainer, M.: A volatility basis set model

779 for summertime secondary organic aerosols over the eastern United States in 2006, J.
780 Geophys. Res. 117, D06301, doi:10.1029/2011JD016831, 2012.

781 Beniston, M., Stephenson, D.B., Christensen, O.B., Ferro, C.A.T., Frei, C., Goyette, S.,
782 Halsnaes, K., Holt, T., Jylha, K., Koffi, B., Palutikof, J., Scholl, R., Semmler, T. and Woth,
783 K.: Future extreme events in European climate: an exploration of regional climate model
784 projections, *Clim. Change*, 81, 71 – 95, doi: 10.1007/s10584-006-9226-z, 2007.

785 Bennartz, R.: Global assessment of marine boundary layer cloud droplet number concentration
786 from satellite, *J. Geophys. Res-Atmos*, 112(D2), D02201, doi:10.1029/2006JD007547, 2007.

787 Brunner, D., Savage, N., Jorba, O., Eder, B., Giordano, L., Badia, A., Balzarini, A., Baro, R.,
788 Bianconi, R., Chemel, C., Curci, G., Forkel, R., Jimenez-Guerrero, P., Hirtl, M., Hodzic, A.,
789 Hozak, L., Im, U., Knote, C., Makar, P., Manders-Groot, A., van Meijgaard, E., Neal, L.,
790 Perez, J.L., Pirovano, G., San Jose, R., Schroder, W., Sokhi, R.S., Syrakov, D., Torian, A.,
791 Tuccella, P., Werhahn, J., Wolke, R., Yahya, K., Zabkar, R., Zhang, Y., Hogrefe, C. and
792 Galmarini, S.: Comparative analysis of meteorological performance of coupled chemistry-
793 meteorology models in the context of AQMEII phase 2, *Atmos. Environ.*, in press,
794 doi:10.1016/j.atmosenv.2014.12.032, 2014.

795 Caldwell, P., H.-N.S. Chin, D.C. Bader, and G. Bala (2009), Evaluation of a WRF dynamical
796 downscaling simulation over California, *Clim. Change.*, 95, 499-521.

797 Campbell, P. C., Zhang, Y., Yahya, K., Wang, K., Hogrefe, C., Pouliot, G., Knote, C., Hodzic,
798 A., San Jose, R., Perez, J., Jimenez-Guerrero, P., Baro, R. and Makar, P.: A Multi-Model
799 Assessment for the 2006 and 2010 Simulations under the Air Quality Model Evaluation
800 International Initiative (AQMEII) Phase 2 over North America: Part I, Indicators of the

801 Sensitivity of O₃ and PM_{2.5} Formation Regimes, Atmos. Environ., in press,
802 doi:10.1016/j.atmosenv.2014.12.026, 2014.

803 Chen, F. and Dudhia, J.: Coupling an advanced land-surface/hydrology model with the Penn
804 State/NCAR MM5 modeling system. Part I: Model implementation and sensitivity. Mon.
805 Wea. Rev., 129, 569-585, 2001.

806 Clough, S.A., Shephard, M.W., Mlawer, J.E., Delamere, J.S., Iacono, M.J., Cady-Pereira, K.,
807 Boukabara, S. and Brown, P.D.: Atmospheric radiative transfer modeling: a summary of the
808 AER codes, J. Quant. Spectrosc. Radiat. Transfer, 91(2), 233 – 244, doi:
809 10.1016/j.qsrt.2004.05.058, 2005.

810 Cooper, O.R., Parrish, D.D., Ziemke, J., Balashov, N.V., Cupeiro, M., Galbally, I.E., Gilge, S.,
811 Horowitz, L., Jensen, N.R., Lamarque, J.-F., Naik, V., Oltmans, S.J., Schwab, J., Shindell,
812 D.T., Thompson, A.M., Thouret, V., Wang, Y. and Zbinden, R.M.: Global distribution and
813 trends of tropospheric ozone: An observation-based review, Elem. Sci. Anth., 2, 000029,
814 doi:10.12952/journal.elementa.000029, 2014.

815 Dasari, H.P., Salgado, R., Perdigo, J. and Challa, V.S.: A regional climate simulation study
816 using WRF-ARW model over Europe and evaluation for extreme temperature weather
817 events, Intl. J. of Atmos. Sci., ID 704079, doi:10.1155/2014/704079, 2014.

818 Ek, M.B., Mitchell, K.E., Lin, Y., Rogers, E., Grunmann, P., Koren, V., Gayno, G. and Tarpley,
819 J.D.: Implementation of NOAA land surface model advances in the National Centers for
820 Environmental Prediction operational mesoscale model, J. Geophys. Res., 108, D22, 8851,
821 doi:10.1029/2002JD003296, 2003.

822 EPA.: Our Nation's Air – Status and Trends through 2010, Particle Pollution, Report by the U.S.
823 EPA, 4pp, <http://www.epa.gov/airtrends/2011>, 2011, last accessed July 6th, 2015.

824 Fan, F., Bradley, R.S. and Rawlins, M.A.: Climate change in the northeastern U.S.: regional
825 climate validation and climate change projections, *Clim. Dyn.*, 43, 145 – 161,
826 doi:10.1007/s00382-014-2198-1, 2014.

827 Feser, F., Rockel, B., Von Storch, H., Winterfeldt, J. and Zahn, M.: Regional climate models add
828 value to global model data, *Bull. Amer. Meteor. Soc.*, 92, 1181 – 1192, 2011.

829 Flato et al.: Evaluation of Climate Models, In: *Climate Change 2013: The Physical Science*
830 *Basis. Contribution of Working Group I to the Fifth Assessment Report of the*
831 *Intergovernmental Panel on Climate Change* [Stocker, T.F., D. Qin, G.-K. Plattner, M.
832 Tignor, S.K. Allen, J. Boschung, A. Nauels, Y. Xia, V. Bex and P.M. Midgley (eds.)],
833 Cambridge University Press, Cambridge, United Kingdom and New York, NY, U.S.A.,
834 2013.

835 Gao, Y., Fu, J.S., Drake, J.B., Liu, Y. and Lamarque, J.F.: Projected changes of extreme weather
836 events in the eastern United States based on a high resolution climate modeling system,
837 *Environ. Res. Lett.*, 7, 044025, 2012.

838 Gao, Y., Fu, J.S., Drake, J.B., Lamarque, J.-F. and Liu, Y.: The impact of emission and climate
839 change on ozone in the United States under representative concentration pathways (RCPs),
840 *Atmos. Chem. Phys.*, 2013, 9607 – 9621, 2013.

841 Glotfelty, T., He, J. and Zhang, Y.: Updated organic aerosol treatments in CESM/CAM5:
842 development and initial application, in preparation, 2015.

843 Gong, S., Barrie, L.A. and Blanchet, J.P.: Modeling sea salt aerosols in the atmosphere: 1. Model
844 development, *J. Geophys. Res.*, 102, 3805-3818, doi:10.1029/96JD02953, 1997.

845 Grell, G.A., Knoche, R., Peckham, S.E. and McKeen, S.A.: Online versus offline air quality
846 modeling on cloud-resolving time scales, *Geophys. Res. Lett.*, 31 (16),
847 doi:10.1029/2004GL020175, 2004.

848 Grell, G.A., Peckham, S.E., Schmitz, R., McKeen, S.A., Frost, G., Skamarock, W.C. and Eder,
849 B.: Fully coupled “online” chemistry within the WRF model, *Atmos. Environ.*, 39, 6957-
850 6975, 2005.

851 Grell, G.A. and Freitas, S.R.: A scale and aerosol aware stochastic convective parameterization
852 for weather and air quality modeling, *Atmos. Chem. Phys.*, 14, 5233-5250, doi:10.5914/acp-
853 14-5233-2014, 2014.

854 Guenther, A., Kart, T., Harley, P., Wiedinmyer, C., Palmer, P.I. and Geron, C.: Estimates of
855 global terrestrial isoprene emissions using MEGAN (Model of Emissions of Gases and
856 Aerosols from Nature), *Atmos. Chem. Phys.*, 6, 3181-3210, 2006.

857 He, J., Zhang, Y., Glotfelty, T., He, R., Bennartz, R., Rausch, J. and Sartelet, K.: Decadal
858 simulation and comprehensive evaluation of CESM/CAM5.1 with advanced chemistry,
859 aerosol microphysics and aerosol-cloud interactions, *J. Adv. Model. Earth Syst.*, 7, 110 –
860 141, doi:10.1002/2014MS000360, 2015.

861 Hong, S.-Y., Noh, Y. and Dudhia, J.: A new vertical diffusion package with an explicit treatment
862 of entrainment processes, *Mon. Wea. Rev.*, 134, 2318-2341, 2006.

863 Hong, S.-Y.: A new stable boundary-layer mixing scheme and its impact on the simulated East
864 Asian summer monsoon, *Q.J.R. Meteorol. Soc.*, 136, 1481 – 1496, doi:0.1002/qj.665, 2010.

865 Hurrell, J.W., Holland, M.M., Gent, P.R., Ghan, S., Kay, J.E., Kushner, P.J., Lamarque, J.-F.,
866 Large, W.G., Lawrence, D., Lindsay, K., Lipscomb, W.H., Long, M.C., Mahowald, N.,
867 Marsh, D.R., Neale, R.B., Rasch, P., Vavrus, S., Vertenstein, M., Bader, D., Collins, W.D.,

868 Hack, J.J., Kiehl, J. and Marshall, S.: The Community Earth System Model: A framework for
869 collaborative research, *Bull. Am. Meteorol. Soc.*, 94, 1339 – 1360, doi:10.1175/BAMS-D-
870 12-00121.1, 2013.

871 Iacono, M.J., Delamere, J.S., Mlawer, E.J., Shepard, M.W., Clough, S.A. and Collins, W.D.:
872 Radiative forcing by long-lived greenhouse gases: Calculations with the AER radiative
873 transfer models, *J. Geophys. Res.*, 113, D13103, doi:10.1029/2008JD009944, 2008.

874 IPCC : Climate change 2013: the physical science basis. In: Stocker, T.F., Qin, D., Plattner, G.-
875 K., Tignor, M.M.B., Allen, S.K., Boschung, J., Nauels, A., Xia, Y., Bex, V., Midgley, P.M.
876 (Eds.), *Contribution of Working Group I to the Fifth Assessment Report of the*
877 *Intergovernmental Panel on Climate Change, Summary for Policymakers*, 2013.

878 Jacob, D., Barring, L., Christensen, O.B., Christensen, J.H., de Castro, M., Deque, M., Giorgi, F.,
879 Hagemann, S., Hirschi, M., Jones, R., Kjellstrom, E., Lenderink, G., Rockel, B., Sanchez, E.,
880 Schar, C., Seneviratne, S.I., Somot, S., van Ulden, A. and van den Hurk, B.: An inter-
881 comparison of regional climate models for Europe: model performance in present-day
882 climate, *Clim. Change*, 81, 31 – 52, 2007.

883 Jimenez, P.A. and Dudhia, J.: Improving the representation of resolved and unresolved
884 topographic effects on surface wind in the WRF model, *J. Appl. Meteor. Climatol.*, 51, 300 –
885 316, 2012.

886 Jones, R.G., Noguer, M., Hassell, D.C., Hudson, D., Wilson, S.S., Jenkins G.J. and Mitchell,
887 J.F.B.: *Generating high resolution climate change scenarios using PRECIS*, Met Office
888 Hadley Centre, Exeter, UK, 40 pp., April 2004, 2004.

889 Jones, S. and Creighton, G.: *AFWA dust emission scheme for WRF/Chem-GOCART*, 2011
890 WRF workshop, June 20-24, Boulder, CO, USA, 2011.

891 Karamchandani, P., Zhang, Y., Chen, S.-Y., and Balmori-Bronson, R.: Development of an
892 extended chemical mechanism for global-through-urban applications, *Atmos. Poll. Res.*, 3, 1
893 – 24, doi:10.5094/apr.2011.047.

894 Kim, J., Waliser, D.E., Mattmann, C.A., Mearns, L.O., Goodale, C.E., Hart, A.F., Crichton,
895 D.J., McGinnis, S., Lee, H., Loikith, P.C. and Boustani, M.: Evaluation of the surface
896 climatology over the conterminous United States in the North American Regional Climate
897 Change Assessment Program Hindcast Experiment using a regional climate model evaluation
898 system, *J. Climate*, 26, 5698 – 5715, 2013.

899 King, N.J., Bower, K.N., Crosier, J. and Crawford, I.: Evaluating MODIS cloud retrievals with in
900 situ observations from VOCALS-REx, *Atmos. Chem. Phys.*, 13, 191 – 209, 2013.

901 Legates, D.R. and McCabe Jr., G.J.: Evaluating the use of “goodness-of-fit” measures in
902 hydrologic and hydroclimatic model validation, *Water Resour. Res.*, 35(1), 233 – 241,
903 doi:10.1029/1998WR900018, 1999.

904 Levy, R.C., Remer, L.A. and Dubovik, O.: Global aerosol optical properties and application to
905 Moderate Resolution Imaging Spectroradiometer aerosol retrieval over land, *J. Geophys.*
906 *Res.*, 112(D13), doi:10.1029/2006JD007815, 2007.

907 Levy, R.C., Mattoo, S., Muchak, L.A., Remer, L.A., Sayer, A.M., Patadia, F., Hsu, N.C.: The
908 Collection 6 MODIS aerosol products over land and ocean, *Atmos. Meas. Tech.*, 6, 2989 –
909 3034, 2013.

910 Leung, R.L., Qian, Y. and Bian, X.: Hydroclimate of the Western United States based on
911 Observations and Regional Climate Simulation of 1981 – 2000, Part I: Seasonal Statistics, *J.*
912 *Clim.*, 16(12), 1892 – 1911, 2003.

913 Liu, X., Easter, R.C., Ghan, S.J., Zaveri, R., Rasch, P., Shi, X., Lamarque, J.-F., Gettelman, A.,
914 Morrison, H., Vitt, F., Conley, A., Park, S., Neale, R., Hannay, C., Ekman, A.M.L., Hess, P.,
915 Mahowald, N., Collins, W., Iacono, M.J., Bretherton, C.S., Flanner, M.G., and Mitchell, D.:
916 Toward a minimal representation of aerosols in climate models: description and evaluation in
917 the Community Atmosphere Model CAM5, *Geosci. Mod. Dev.*, 5, 709 – 739,
918 doi:10.5194/gmd-5-709-2012, 2012.

919 Loeb, N.G., Wielicki, B.A., Doelling, D.R., Smith, L., Keyes, D.F., Kato, S., Manalo-Smith, N.
920 and Wong, T.: Toward Optimal Closure of the earth’s top-of-atmosphere radiation budget, *J.*
921 *Climate*, 22, 748 – 766, 2009.

922 Ma, P.-L., Rasch, P.J., Fast, J.D., Easter, R.C., Gustafson Jr., W.I., Liu, X., Ghan, S.J. and Singh,
923 B.: Assessing the CAM5 physics suite in the WRF-Chem model: implementation, resolution
924 sensitivity, and a first evaluation for a regional case study, *Geosci. Model Dec.*, 7, 755 – 778,
925 2014.

926 Mass, C.: Improved subgrid drag or hyper PBL/vertical resolution? Dealing with the stable PBL
927 problems in WRF, presented at the 13th WRF Users’ Workshop, June 26 – 29, Boulder, CO,
928 2012.

929 Molders, N., Bruyere, C.L., Gende, S. and Pirhala, M.A.: Assessment of the 2006-2012
930 Climatological Fields and Mesoscale Features from Regional Downscaling of CESM Data by
931 WRF/Chem over Southeast Alaska, *Atmos. Clim. Sci.*, 4, 589 – 613, 2014.

932 Morrison, H., Thompson, G. and Tatarskii, V.: Impact of cloud microphysics on the development
933 of trailing stratiform precipitation in a simulated squall line: Comparison of One- and Two-
934 Moment Schemes, *Mon. Wea. Rev.*, 137, 991-1007, 2009.

935 Moss, R. H., Edmonds, J.A., Hibbard, K.A., Manning, M.R., Rose, S.K., van Vuuren, D.P.,
936 Carter, T.R., Emori, S., Kainuma, M., Kram, T., Meehl, G.A., Mitchell, J.F.B., Nakicenovic,
937 N., Riahi, K., Smith, S.J., Stouffer, R.J., Thomson, A.M., Weyant, J.P. and Wilbanks, T.J.:
938 The next generation of scenarios for climate change research and assessment, *Nature*, 463,
939 747 – 756, doi: 10.1038/nature0882, 2010.

940 Nasrollahi, N., AghaKouchak, A., Li, J., Gao, X., Hsu, K. and Sorooshian, S.: Assessing the
941 Impacts of Different WRF Precipitation Physics in Hurricane Simulations, *Wea. Forecasting*,
942 27, 1003 – 1016, 2012.

943 Neale R.B., Jadwiga, H.R., Conley, A.J., Park, S., Lauritzen, P.H., Gettelman, A., Williamson,
944 D.L., Rasch, P., Vavrus, S.J., Taylor, M.A., Collins, W.D., Zhang, M. and Lin, S.-J.:
945 Description of the NCAR Community Atmosphere Model (CAM 5.0), NCAR Tech. Note
946 NCAR/TN-486+STR, Natl. Cent. for. Atmos. Res., Boulder, CO, available at
947 http://www.cesm.ucar.edu/models/cesm1.0/cam/docs/description/cam5_desc.pdf, 2010, last
948 accessed July 6th, 2015.

949 Otte, T.L., Nolte, C.G., Otte, M.J. and Bowden, J.H.: Does Nudging squelch the extremes in
950 regional climate modeling? *J. Clim.*, 25, 7046 – 7066, doi:10.1175/JCLI-D-12-00048.1,
951 2012.

952 Penrod, A., Zhang, Y., Wang, K., Wu, S-Y. and Leung, R.L.: Impacts of future climate and
953 emission changes on U.S. air quality, *Atmos. Environ.*, 89, 533 – 547, 2014.

954 Petikainen, J.-P., O'Donnell, D., Teichmann, C., Karstens, U., Pfeifer, S., Kazil, J., Podzun, R.,
955 Fiedler, S., Kokkola, H., Birmili, W., O'Dowd, C., Baltensperger, U., Weingartner, E.,
956 Gehrig, R., Spindler, G., Kulmala, M., Feichter, J., Jacob, D. and Laaksonen, A.: The
957 regional aerosol-climate model REMO-HAM, *Geosci. Mod. Dev.*, 5, 1323 – 1339, 2012.

958 Pleim, J.E. and Gilliam, R.: An indirect data assimilation scheme for deep soil temperature in the
959 Pleim-Xiu Land Surface Model, *J. Appl. Meteor. Climatol.*, 48, 1362 – 1376, 2009.

960 Pouliot, G., van der Gon, H.A.C.D., Kuenen, J., Zhang, J., Moran, M. and Makar, P.: Analysis of
961 the Emission Inventories and Model-Ready Emission Datasets of Europe and North America
962 for Phase 2 of the AQMEII Project, *Atmos. Environ.*, in press,
963 doi:10.1016/j.atmosenv.2014.10.061, 2014.

964 Rawlins, M.A., Bradley, R.S. and Diaz, H.F.: Assessment of regional climate model simulation
965 estimates over the northeast United States, *J. Geophys. Res.*, 117, D23112,
966 doi:10.1029/2012JD018137, 2012.

967 Refslund, J., Dellwik, E., Hahmann, A.N., Barlage, M.J. and Boegh, E.: Development of satellite
968 green vegetation fraction time series for use in mesoscale modeling: application to the
969 European heat wave 2006, *Theor. Appl. Climatol.*, 117, 377-392, doi:10.1007/s00704-013-
970 1004-z, 2014.

971 Sarwar, G., Luecken, D.J. and Yarwood, G.: Developing and implementing an updated chlorine
972 chemistry into the Community Multiscale Air Quality Model, presented at the 28th
973 NATO/CCMS International Technical Meeting, Leipzig, Germany, May 15 – 19, 2006.

974 Sarwar, G., Luecken, D. and Yarwood, G.: Chapter 2.9: Developing and implementing an
975 updated chlorine chemistry into the community multiscale air quality model, *Developments*
976 *in Environmental Science*, Volume 6, C. Borrego and E. Renner (Eds.), Elsevier Ltd,
977 DOI:10.1016/S1474-8177(07)06029-9, 168 pp., 2007.

978 Sarwar, G., Fahey, K., Napelenok, S., Roselle, S. and Mathur, R.: Examining the impact of
979 CMAQ model updates on aerosol sulfate predictions, the 10th Annual CMAS Models-3
980 User's Conference, October, Chapel Hill, NC, 2011.

981 Shan, Z., Parol, F., Riedi, J., Cornet, C. and Thieuleux, F.: Examination of POLDER/PARASOL
982 and MODIS/Aqua cloud fractions and properties representativeness, *J. Climate*, 24, 4435 –
983 4450, 2011.

984 Sievering, H.: Small-particle dry deposition under high wind speed conditions: Eddy flux
985 measurements at the boulder atmospheric observatory, *Atmos. Environ.*, 21 (10), 2179 –
986 2185, 1987.

987 Tewari, M., Chen, F., Wang, W., Dudhia, J., LeMone, M.A., Mitchell, K., Ek, M., Gayno, G.,
988 Wegiel, J. and Cuenca, R.H.: Implementation and verification of the unified NOAH land
989 surface model in the WRF model. 20th conference on weather analysis and forecasting/16th
990 conference on numerical weather prediction, pp. 11 – 15, 2004.

991 Toth, T.D., Zhang, J., Campbell, J.R., Reid, J.S., Shi, Y., Johnson, R.S., Smirnov, A., Vaughan,
992 M.A. and Winker, D.M.: Investigating enhanced Aqua MODIS aerosol optical depth
993 retrievals over the mid-to-high latitude Southern Oceans through intercomparison with co-
994 located CALIOP, MAN and AERONET data sets, *J. Geophys. Res: Atmos*, 18, 1- 15, 2013.

995 van Vuuren, D.P., Edmonds, J., Kainuma, M., Riahi, K., Thomson, A., Hibbard, K., Hurtt, G.C.,
996 Kram, T., Krey, V., Lamarque, J.-F., Masui, T., Meinshausen, M., Nakicenovic, N., Smith,
997 S.J. and Rose, S.K.: The representative concentration pathways: an overview, *Climate*
998 *Change*, 109, 5 – 31, doi: 10.1007/s10584-011-0148-z, 2011.

999 Wang, K., Zhang, Y., Yahya, K., Wu, S.-Y. and Grell, G.: Implementation and initial
1000 application of new chemistry-aerosol options in WRF/Chem for simulating secondary
1001 organic aerosols and aerosol indirect effects for regional air quality, *Atmos. Environ.*, in
1002 press, doi: 10.1016/j.atmosenv.2014.12.007, 2014a.

1003 Wang, K., Yahya, K., Zhang, Y., Hogrefe, C., Pouliot, G., Knote, C., Hodzic, A., San Jose, R.,
1004 Perez, J.L., Guerrero, P.J., Baro, R. and Makar, P.: Evaluation of Column Variable
1005 Predictions Using Satellite Data over the Continental United States: A Multi-Model
1006 Assessment for the 2006 and 2010 Simulations under the Air Quality Model Evaluation
1007 International Initiative (AQMEII) Phase 2, *Atmos. Environ.*, in press,
1008 doi:10.1016/j.atmosenv.2014.07.044, 2014b.

1009 Warrach-Sagi, K., Schwitalla, T., Wulfmeyer, V. and Bauer, H.-S.: Evaluation of a climate
1010 simulation in Europe based on the WRF-NOAH model system: precipitation in Germany,
1011 *Clim. Dyn.*, 41, 755 – 774, doi:10.1007/s00382-013-1727-7, 2013.

1012 Willmott, C. J.: On the validation of models, *Phys. Geog.*, 2, 184 – 194, 1981.

1013 Xing, J., Mathur, R., Pleim, J., Hogrefe, C., Gan, C.-M., Wong, D.C., Wei, C., Gilliam, R. and
1014 Pouliot, G.: Observations and modeling of air quality trends over 1990-2010 across the
1015 Northern Hemisphere: China, the United States and Europe, *Atmos. Chem. Phys.*, 15, 2723 –
1016 2747, doi:10.5194/acp-15-2723-2015.

1017 Xu, Z. and Yang, Z.-L.: An improved dynamical downscaling method with GCM Bias
1018 Corrections and Its Validation with 30 years of climate simulations, *J. Clim.*, 25, 6271 –
1019 6286, 2012.

1020 Yahya, K., Wang, K., Gudoshava, M., Glotfelty, T. and Zhang, Y.: Application of WRF/Chem
1021 over North America under the AQMEII Phase 2. Part I. Comprehensive Evaluation of 2006
1022 Simulation, *Atmospheric Environment*, in press, doi:10.1016/j.atmosenv.2014.08.063, 2014.

1023 Yahya, K., He, J., and Zhang, Y.: Multi-Year Applications of WRF/Chem over Continental U.S.:
1024 Model Evaluation, Variation Trend, and Impacts of Boundary Conditions over CONUS, *J.*
1025 *Geophys. Res.*, in review, 2015a.

1026 Yahya, K., Wang, K., Zhang, Y. and Kleindienst, T.E.: Application of WRF/Chem over North
1027 America under the AQMEII Phase 2. Part II. Comprehensive Evaluation of 2010 Simulation
1028 and Responses of Air Quality and Meteorology-Chemistry Interactions to Changes in
1029 Emissions and Meteorology from 2006 to 2010, *Geosci. Model Dev.*, in press, 2015b.

1030 Yarwood, G., Rao, S., Yocke, M. and Whitten, G.Z.: Final Report – Updates to the Carbon Bond
1031 Chemical Mechanism: CB05, Rep. RT-04-00675, 246 pp., Yocke and Co., Novato, Calif.,
1032 2005.

1033 Yu, S., Dennis, R., Roselle, S., Nenes, A., Walker, J., Eder, B., Schere, K., Swall, J., and
1034 Robarge, W.: An assessment of the ability of 3-D air quality models with current
1035 thermodynamic equilibrium models to predict aerosol NO₃-, *J. Geophys. Res.*, 110, D07S13,
1036 doi:10.1029/2004JD004718, 2005.

1037 Yu, S., Eder, B., Dennis, R., Chu, S.-H., and Schwartz, S.: New unbiased symmetric metrics for
1038 evaluation of air quality models, *Atmos. Sci. Lett.*, 7, 26 – 34, 2006.

1039 Yu, S., Mathur, R., Pleim, J., Wong, D., Gilliam, R., Alapaty, K., Zhao, C., and Liu, X.: Aerosol
1040 indirect effect on the grid-scale clouds in the two-way coupled WRF-CMAQ: model
1041 description, development, evaluation and regional analysis, *Atmos. Chem. Phys.*, 14, 11247 –
1042 11285, doi:10.5194/acp-14-1-2014, 2014.

1043 Zhang, Y., Liu, P., Pun, B., and Seigneur, C.: A comprehensive performance evaluation of
1044 MM5-CMAQ for summer 1999 Southern Oxidants Study Episode, Part-I. Evaluation
1045 Protocols, Databases and Meteorological Predictions, *Atmos. Environ.*, 40, 4825 – 4838,
1046 2006.

1047 Zhang, Y., Wen, X.-Y. and Jang, C.J.: Simulating chemistry-aerosol-cloud-radiation-climate
1048 feedbacks over the CONUS using the online-coupled Weather Research Forecasting Model
1049 with chemistry (WRF/Chem), Atmos. Environ., 44, 3568 – 3582, 2010.

1050 Zhang, Y., Y.-C. Chen, G. Sarwar, and K. Schere, 2012a, Impact of Gas-Phase Mechanisms on
1051 Weather Research Forecasting Model with Chemistry (WRF/Chem) Predictions: Mechanism
1052 Implementation and Comparative Evaluation, J. Geophys. Res., 117, D1,
1053 doi:10.1029/2011JD015775.

1054 Zhang, Y., P. Karamchandani, T. Glotfelty, D. G. Streets, G. Grell, A. Nenes, F.-Q. Yu, and R.
1055 Bennartz, 2012b, Development and Initial Application of the Global-Through-Urban
1056 Weather Research and Forecasting Model with Chemistry (GU-WRF/Chem), J. Geophys.
1057 Res., 117, D20206, doi:10.1029/2012JD017966.

1058

1059

Table 1. Model configurations and set-up

Model Attribute	Configuration	Reference
Domain and Resolutions	36km × 36km, 148 × 112 horizontal resolution over continental U.S., with 34 layers vertically from surface to 100 hPa	-
Simulation Period	January 2001 to December 2010	-
Chemical and Meteorological ICs/BCs	Downscaled from the modified Community Earth System Model/Community Atmosphere Model (CESM/CAM5) v1.2.2; Meteorological ICs/BCs bias-corrected with National Center for Environmental Protection's Final (FNL) Operational Global Analysis data	He et al. (2014) Glotfelty et al. (2015)
Biogenic Emissions	Model of Emissions of Gases and Aerosols from Nature (MEGAN2)	Guenther et al. (2006)
Dust Emissions	Atmospheric and Environmental Research Inc. and Air Force Weather Agency (AER/AFWA)	Jones and Creighton (2011)
Sea-Salt Emissions	Gong et al. parameterization	Gong et al. (1997)
Radiation	Rapid and accurate Radiative Transfer Model for GCM (RRTMG) SW and LW	Clough et al. (2005) Iacono et al. (2008)
Boundary Layer	Yonsei University (YSU)	Hong et al. (2006) Hong (2010)
Land Surface	National Center for Environmental Prediction, Oregon State University, Air Force and Hydrologic Research Lab (NOAH)	Chen and Dudhia (2001) Ek et al. (2003) Tewari et al. (2004)
Microphysics	Morrison double moment scheme	Morrison et al. (2009)
Cumulus Parameterization	Grell 3D Ensemble	Grell and Freitas (2014)
Gas-phase chemistry	Modified CB05 with updated chlorine chemistry	Yarwood et al. (2005) Sarwar et al. (2006) Sarwar et al. (2007)
Photolysis	Fast Troposphere Ultraviolet Visible (FTUV)	Tie et al. (2003)
Aqueous-phase chemistry	AQ chemistry module (AQCHEM) for both resolved and convective clouds	Based on AQCHEM in CMAQv4.7 of (Sarwar et al. 2011)
Aerosol module	MADE/VBS	Ahmadov et al. (2012)
Aerosol Activation	Abdul-Razzak and Ghan	Abdul-Razzak and Ghan (2000)

Table 2. The 10-year (2001 – 2010) average performance statistics for the simulated meteorological, aerosol, cloud, radiation variables, and chemical species against surface observational networks and satellite retrieval products.

Database and Variable	Mean Obs	Mean Sim	R	MB	NMB (%)	NME (%)
NCDC T2 (°C)	12.5	12.2	1.0	-0.3	-2.6	7.9
NCDC RH2 (%)	68.4	70.8	0.8	2.4	3.5	6.8
NCDC WS10 (m s ⁻¹)	3.54	3.84	0.3	0.3	8.6	28.4
NCDC WD10 (deg)	151.4	180.0	0.2	28.6	18.9	22.0
NADP Precip (mm day ⁻¹)	18.0	26.3	0.5	8.3	45.9	65.1
CERES SWDOWN (W m ⁻²)	184.1	184.6	0.8	0.5	0.3	8.4
CERES GSW (W m ⁻²)	157.5	151.8	0.8	-5.7	-3.6	9.6
CERES GLW (W m ⁻²)	323.3	325.7	1.0	2.4	0.7	1.8
CERES OLR (W m ⁻²)	240.0	224.8	0.6	-15.0	-6.3	6.3
MODIS AOD	0.14	0.10	0.1	-0.03	-24.0	38.5
MODIS CLDFRA	58.3	62.0	0.7	3.7	6.4	11.9
MODIS-derived CDNC (cm ⁻³)	169.8	130.0	0.4	-39.9	-23.5	38.0
MODIS CWP (g m ⁻²)	179.5	170.0	0.3	-9.6	-5.3	61.2
MODIS COT	16.5	9.2	0.2	-7.3	-44.3	54.0
CERES SWCF (W m ⁻²)	-41.8	-49.6	0.5	7.8	18.6	31.4
CERES LWCF (W m ⁻²)	24.8	31.8	0.6	6.9	28.0	34.7
AQS Hourly O ₃ (ppb)	29.3	32.1	0.6	2.8	9.7	22.4
AQS Max 1-hr O ₃ (ppb)	48.9	49.7	0.6	0.8	1.7	7.9
AQS Max 8-hr O ₃ (ppb)	43.7	45.9	0.6	2.2	5.0	9.3
CASTNET Hourly O ₃ (ppb)	35.0	31.9	0.7	-3.1	-8.8	19.8
CASTNET Max-1hr O ₃ (ppb)	47.4	38.5	0.4	-8.9	-18.8	31.4
CASTNET Max 8-hr O ₃ (ppb)	43.3	37.9	0.5	-5.4	-12.5	29.6
AQS 24-hr PM ₁₀ (µg m ⁻³)	22.5	11.0	0.1	-11.5	-51.2	57.1
IMPROVE PM _{2.5} (µg m ⁻³)	5.33	6.57	0.4	1.2	23.3	53.4
STN PM _{2.5} (µg m ⁻³)	12.0	10.7	0.2	-1.3	-10.8	38.3
IMPROVE SO ₄ ²⁻ (µg m ⁻³)	1.45	1.86	0.8	0.4	28.0	41.8
STN SO ₄ ²⁻ (µg m ⁻³)	3.10	3.74	0.7	0.6	20.7	36.8
IMPROVE ¹ NO ₃ ⁻ (µg m ⁻³)	0.54	0.44	0.7	-0.1	-17.9	64.6
STN NO ₃ ⁻ (µg m ⁻³)	1.62	0.70	0.4	-0.9	-56.9	65.3
IMPROVE NH ₄ ⁺ (µg m ⁻³)	1.02	0.72	0.4	-0.3	-29.6	45.5
STN NH ₄ ⁺ (µg m ⁻³)	1.34	1.05	0.5	-0.3	-21.5	38.7
IMPROVE EC (µg m ⁻³)	0.23	0.16	0.6	-0.1	-30.7	48.3
STN EC (µg m ⁻³)	0.65	0.38	0.2	-0.3	-42.0	52.8
IMPROVE OC (µg m ⁻³)	1.10	1.88	0.2	0.8	71.7	134.6
IMPROVE TC (µg m ⁻³)	1.33	2.05	0.2	0.7	53.9	116.3
STN TC (µg m ⁻³)	4.42	2.42	0.1	-2.0	-45.3	69.7

¹ NH₄⁺ IMPROVE data only available up to 2005.

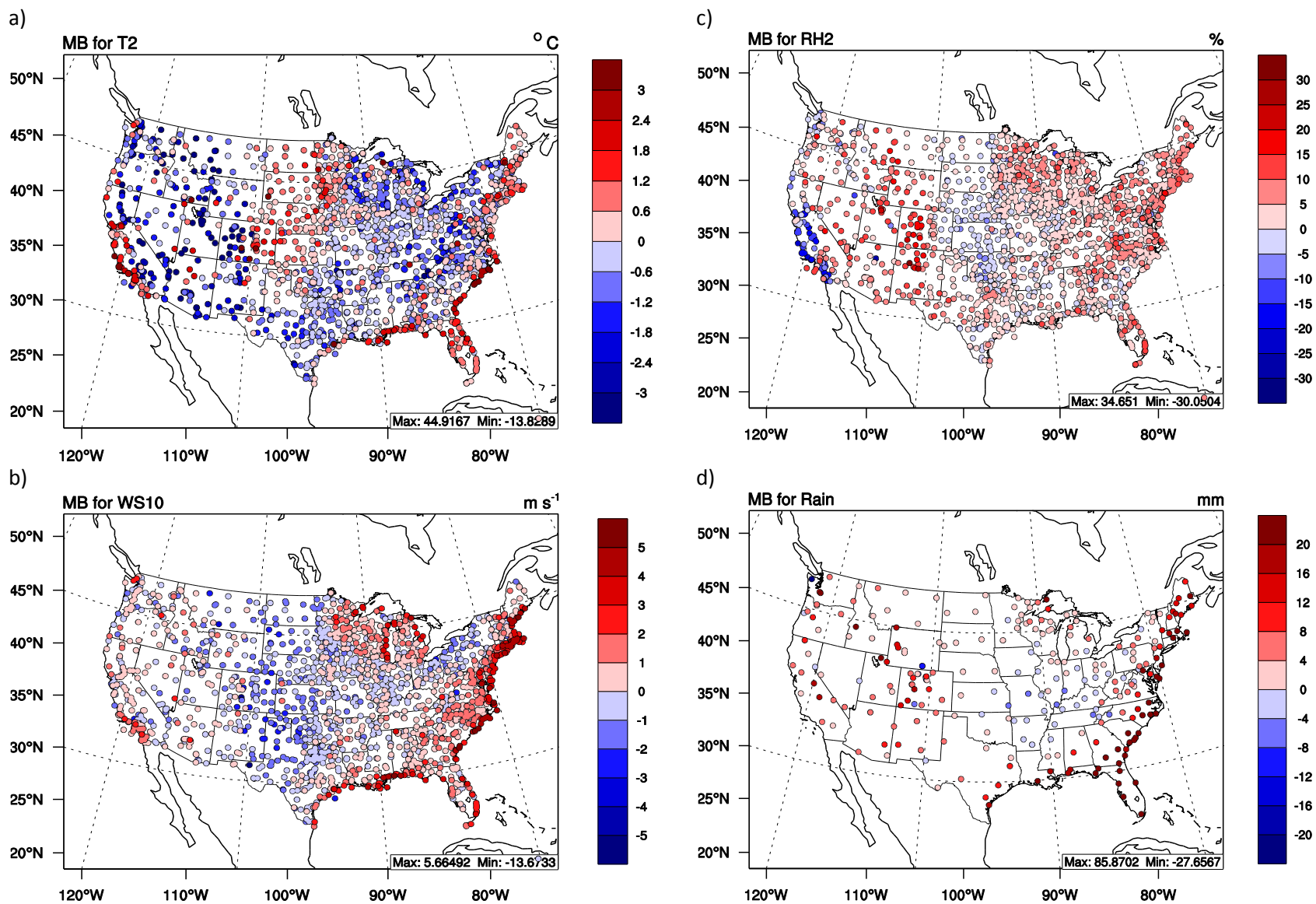


Figure 1. Spatial distribution of MBs for: a) 2-m temperature (T2), b) 2-m relative humidity (RH2), c) 10-m wind speed (WS10) from NCDC, and d) weekly precipitation from NADP. Each marker represents the MB of each variable at each observational site.

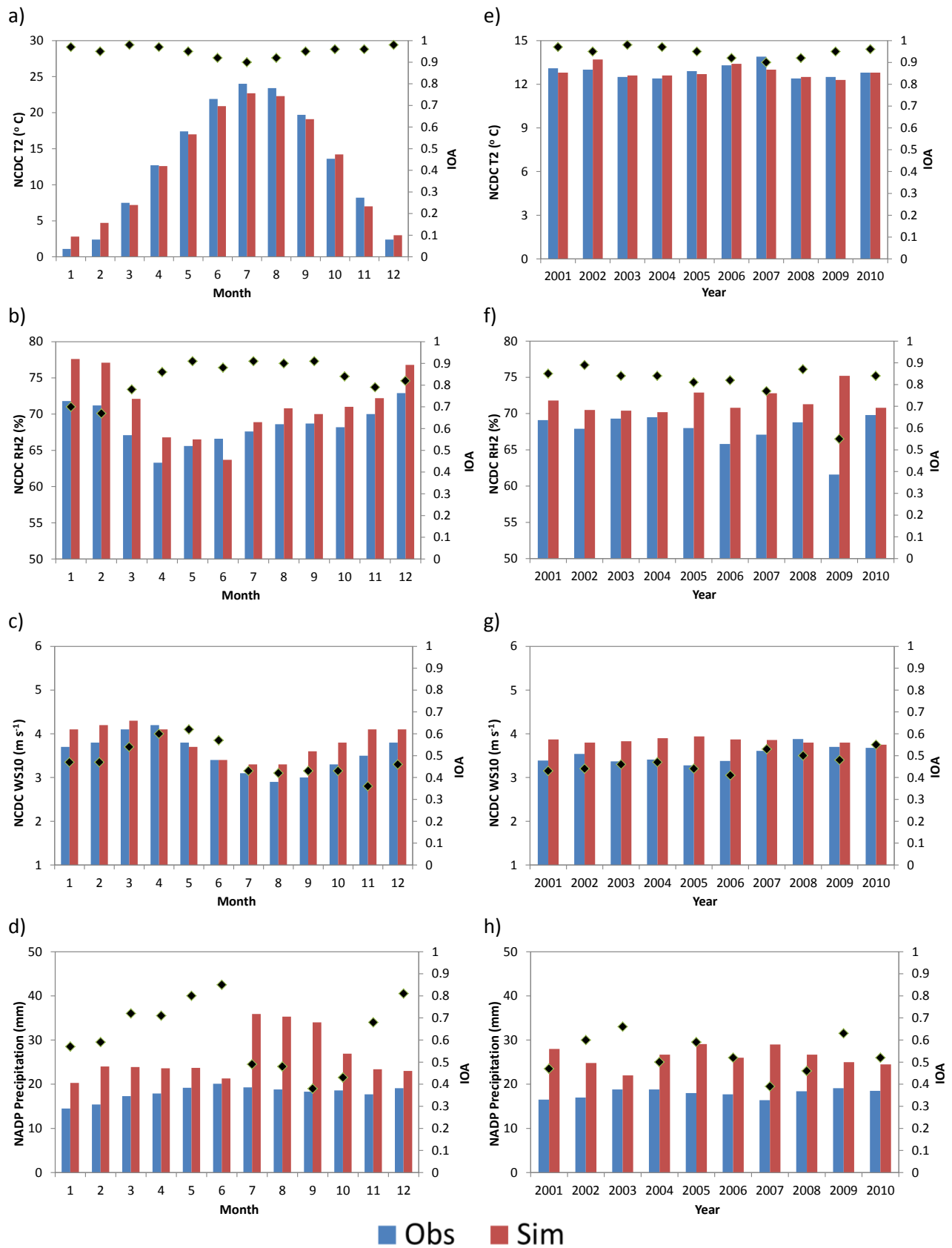


Figure 2. Time series of 10-year averaged monthly observations (blue) versus simulations (red) for: a) T2, b) RH2, and c) WS10 against NCDC data, and d) precipitation against NADP data, and annual averages for e) T2, f) RH2, and g) WS10 against NCDC data, and h) precipitation against NADP. IOA statistics (black diamonds) are also provided on the secondary y-axes in panels a) – h).

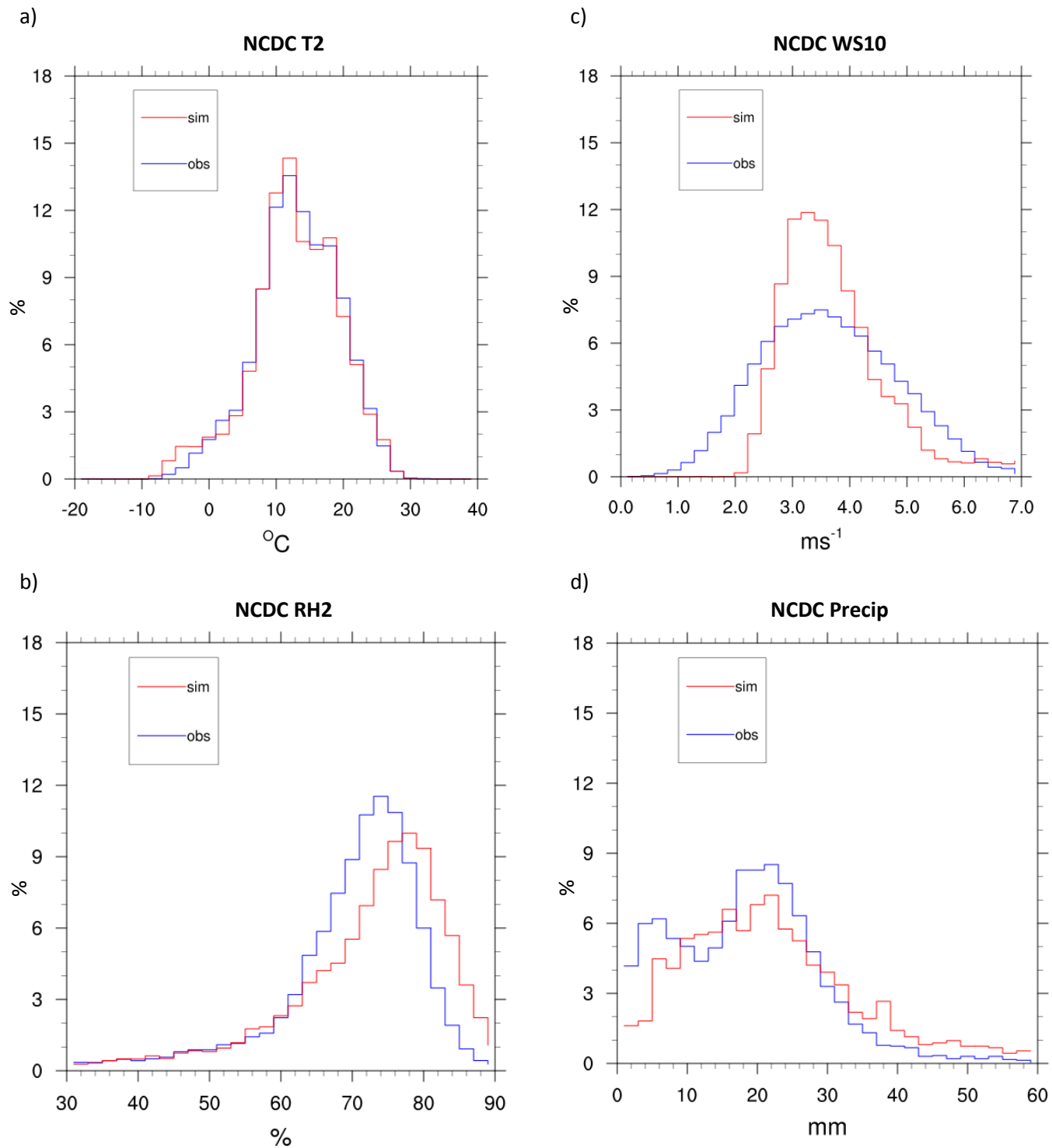


Figure 3. Probability density functions (PDFs) of a) T2, b) RH2, c) WS10 against NCDC, and d) precipitation against NADP for 2001 to 2010 over 30 bins in the respective ranges for all variables.

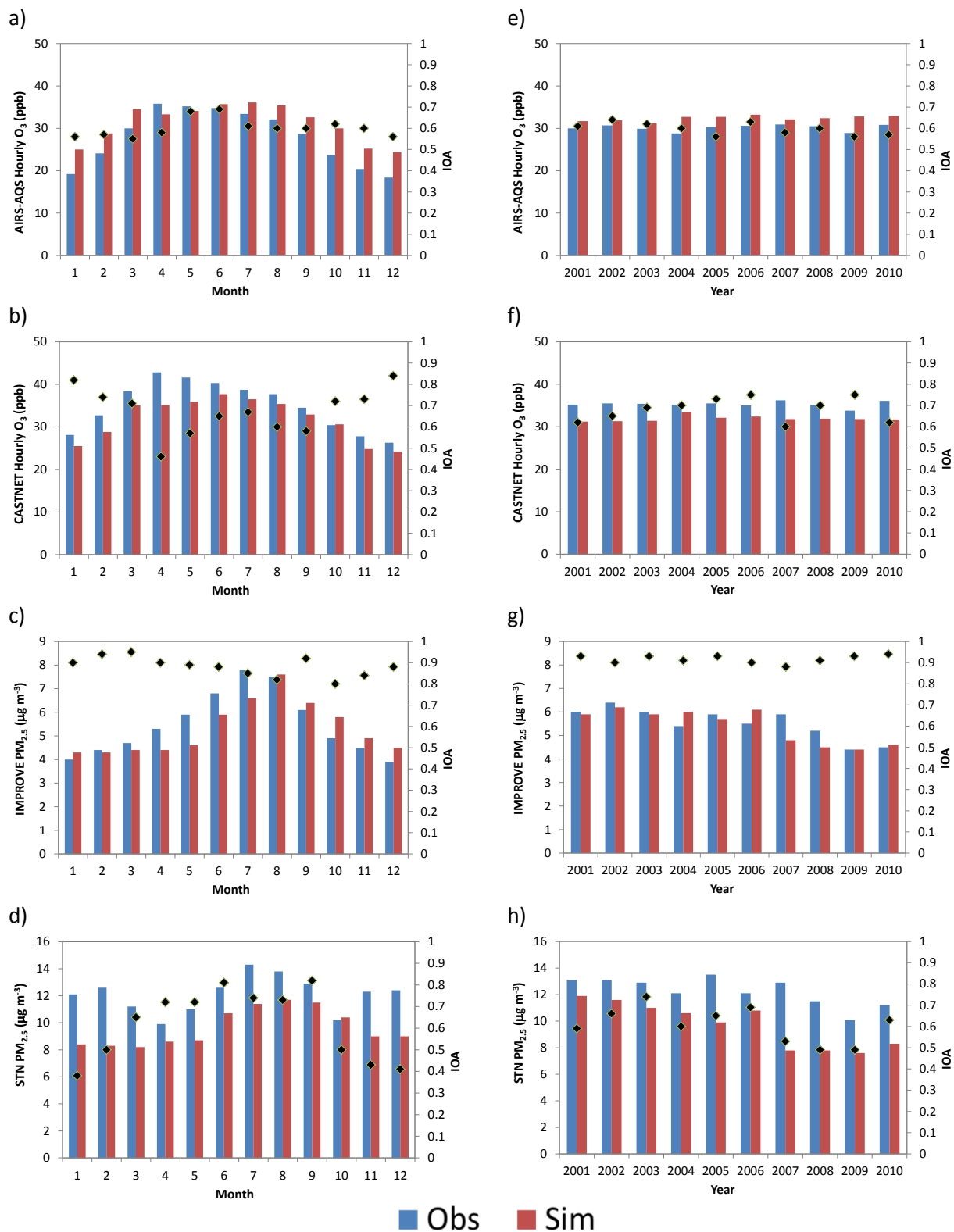


Figure 4. Time series of 10-year averaged monthly-mean observations (blue) versus simulations (red) for: a) O₃ against AQS data, b) O₃ against CASTNET data, c) PM_{2.5} against IMPROVE, and d) PM_{2.5} against STN, and annual averages for e) O₃ against AQS data, f) O₃ against CASTNET data, g) PM_{2.5} against IMPROVE, and h) PM_{2.5} against STN. IOA statistics (black diamonds) are also provided on the secondary y-axes in panels a) – h).

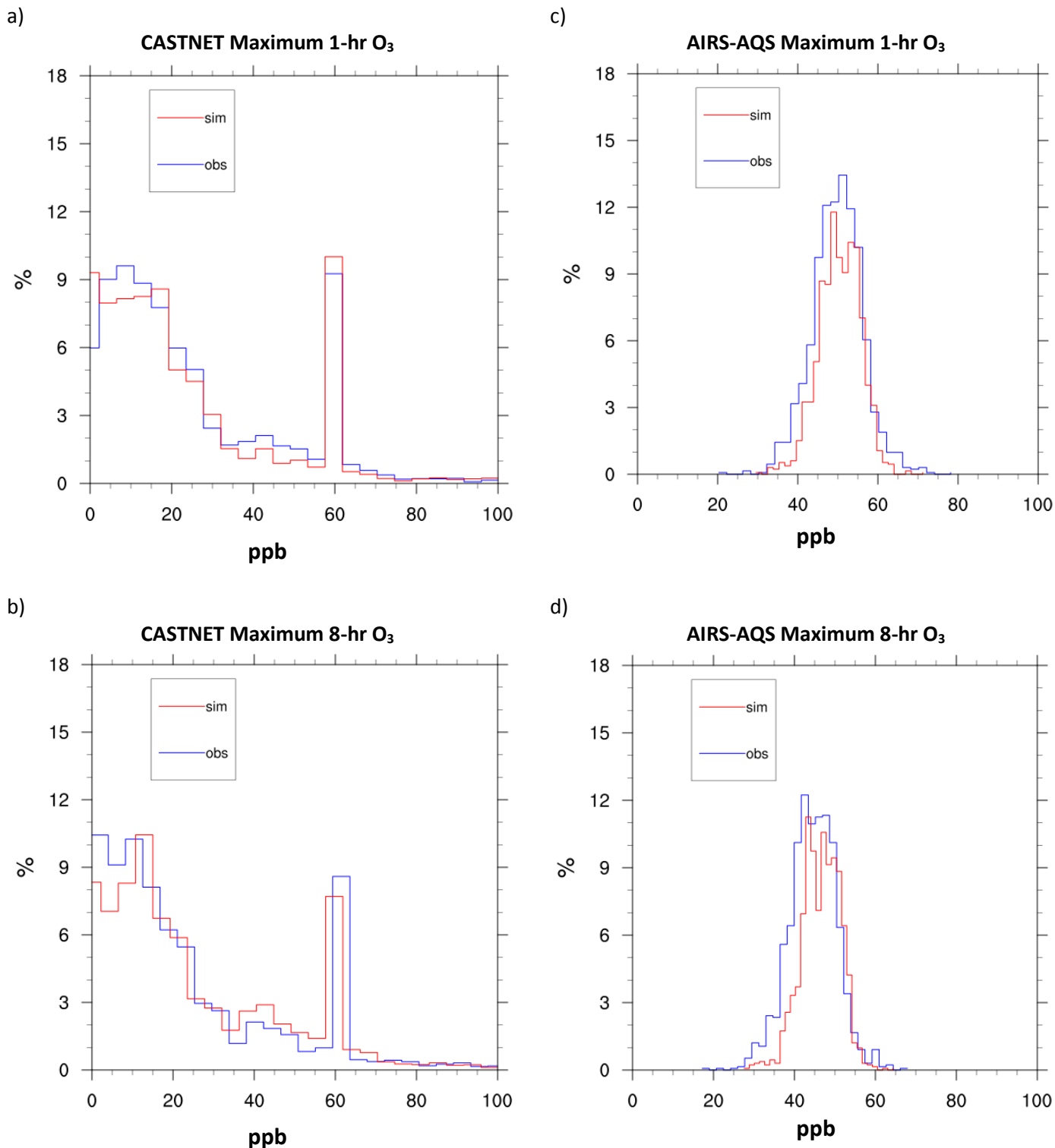


Figure 5. Probability density functions (PDFs) of a) maximum 1-hr O₃ against CASTNET, b) maximum 8-hr O₃ against CASTNET, c) maximum 1-hr O₃ against AIRS-AQS, and d) maximum 8-hr O₃ against AIRS-AQS for 2001 to 2010 over 30 bins in the respective ranges for all variables.

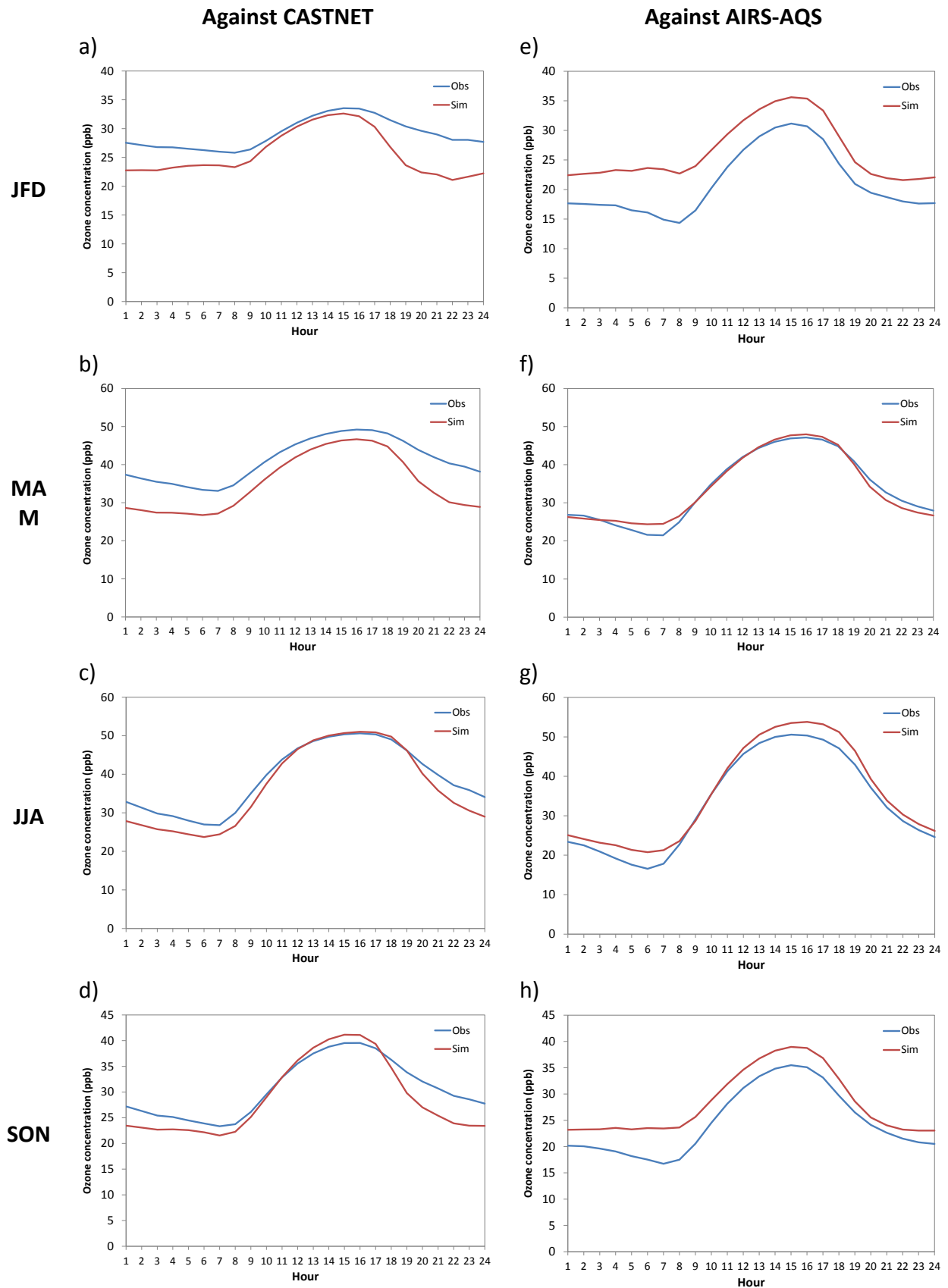


Figure 6. Diurnal variation of observed vs. simulated hourly O_3 concentrations against CASTNET (left column from a) to d)) and AIRS-AQS (right column from e) to h)) for all climatological seasons. The x-axes refer to hours in local standard time.

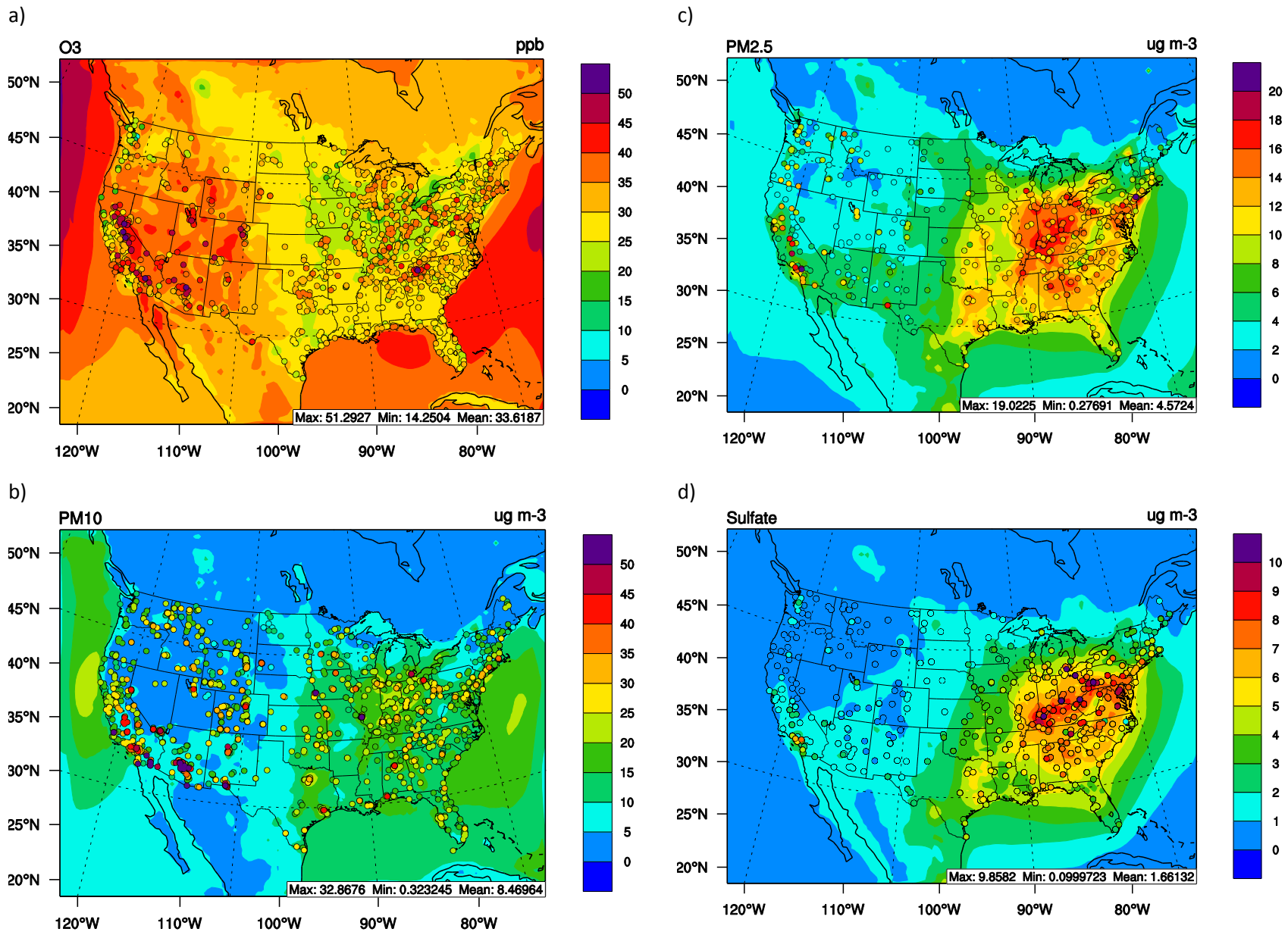


Figure 7. Spatial distribution of 10-year averaged hourly observed vs. simulated a) O₃ for CASTNET and AIRS-AQS, b) PM₁₀ from AIRS-AQS, c) PM_{2.5}, and d) PM_{2.5} sulfate from STN and IMPROVE. The background plots represent the simulated data while observations are represented by the markers.

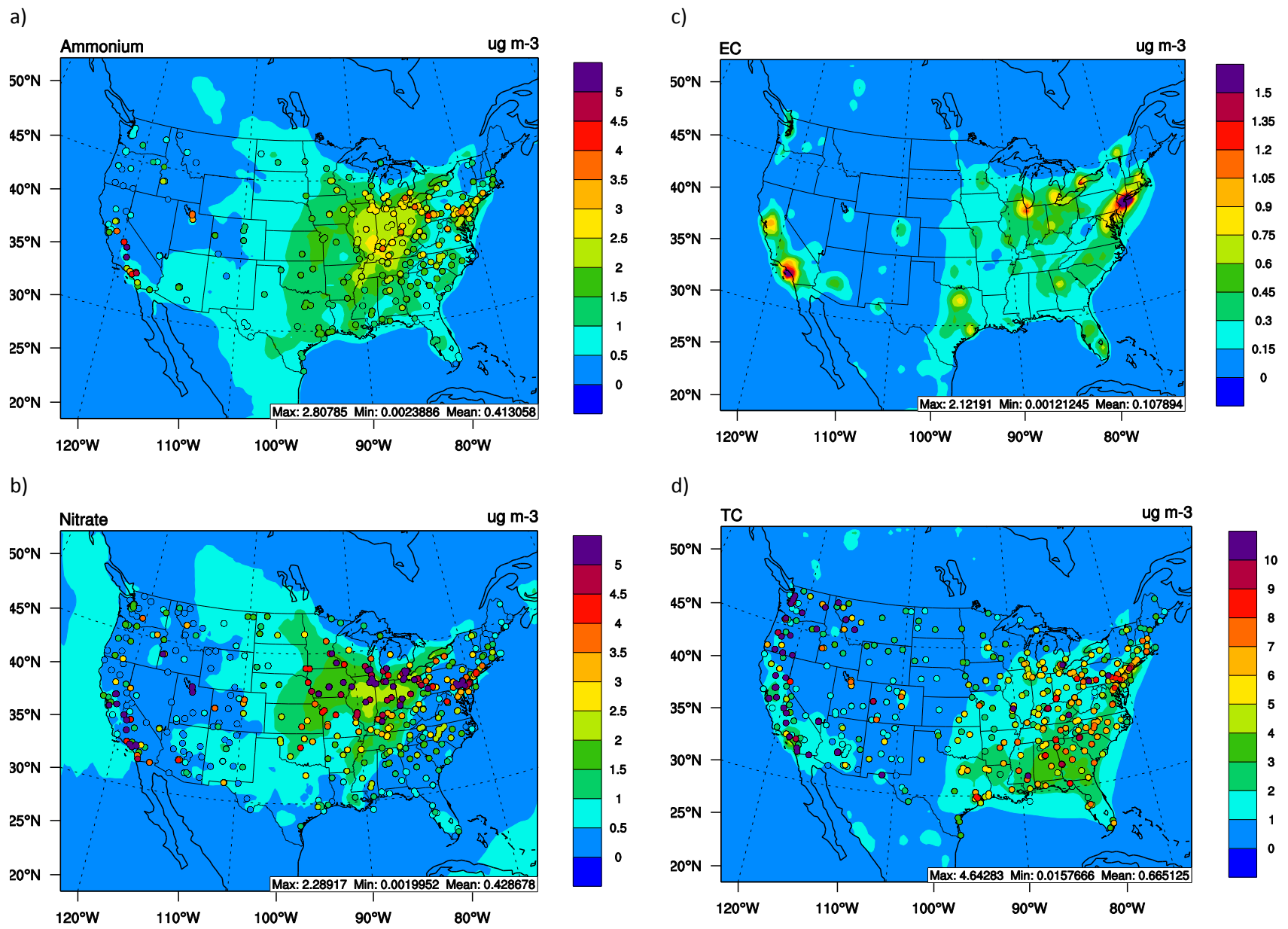


Figure 8. Spatial distribution of 10-year averaged hourly observed vs. simulated a) Ammonium, b) Nitrate, c) EC, and d) TC from STN and IMPROVE. The background plots represent the simulated data while observations are represented by the markers.

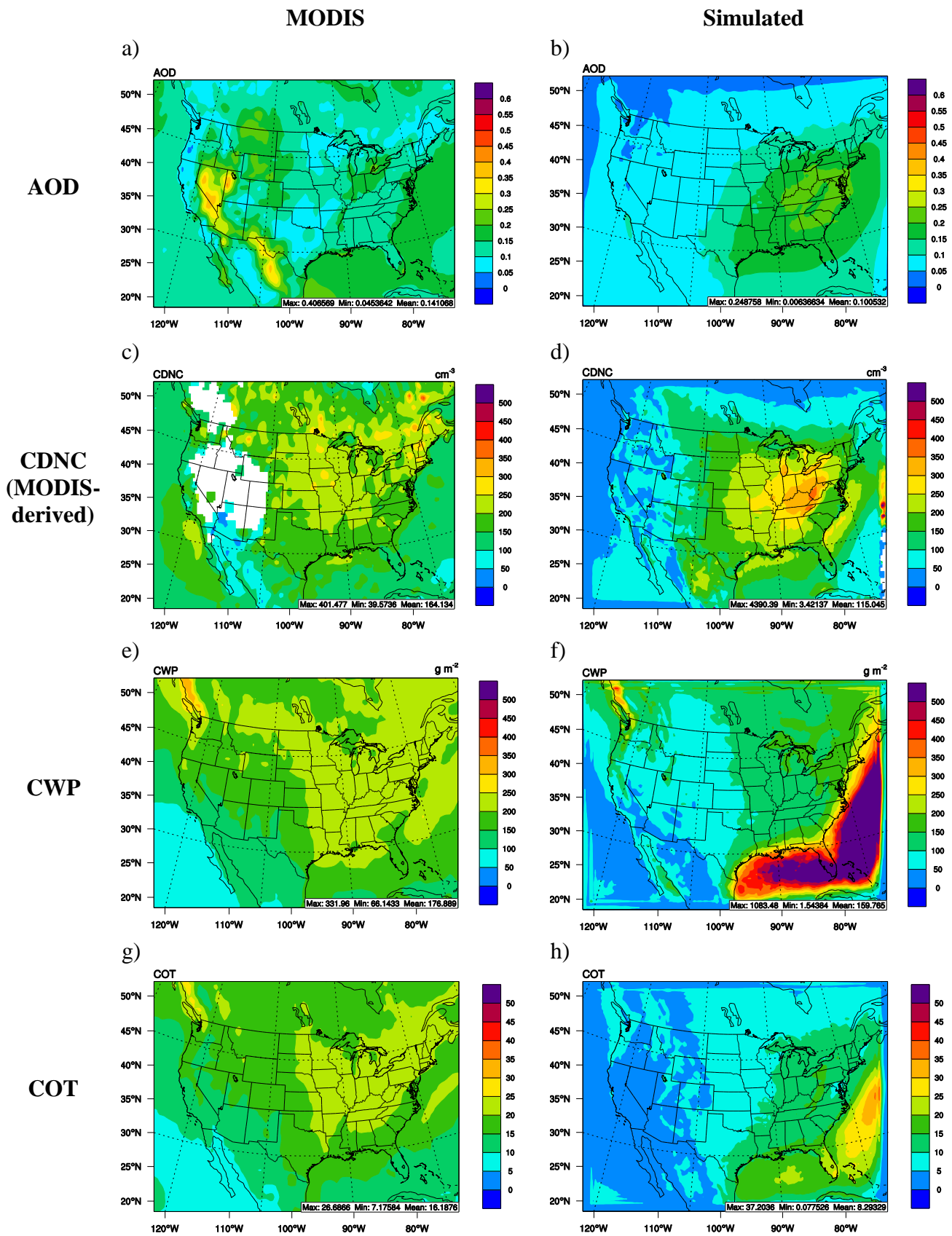


Figure 9. 10-year averaged MODIS (left) vs. simulated (right) AOD (a and b), CDNC (c and d), CWP (e and f), and COT (f and g).

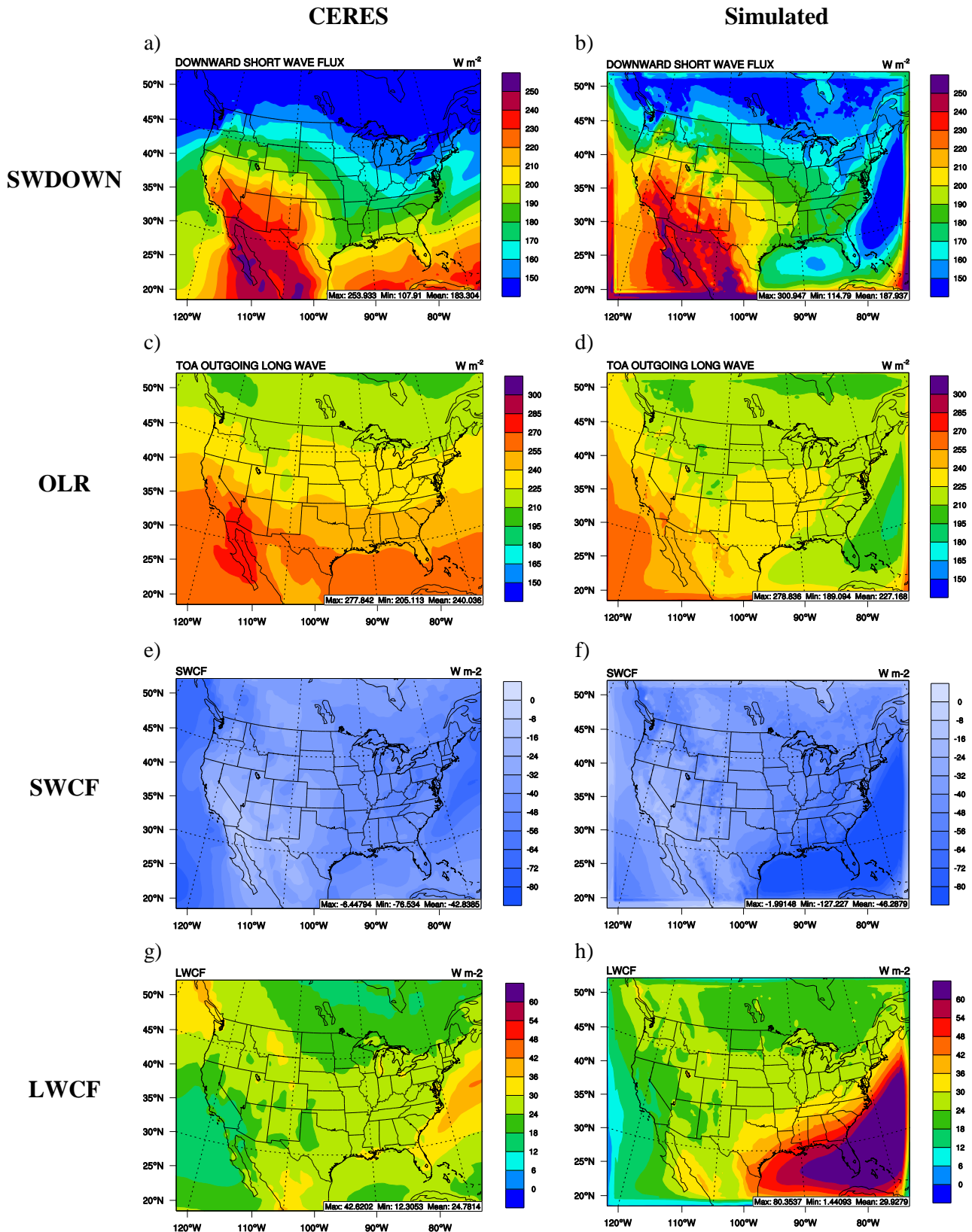


Figure 10. 10-year averaged CERES (left) vs. simulated (right) SWDOWN (a and b), OLR (c and d), SWCF (e and f), and LWCF (f and g).